Validation of carbon isotopologue distribution measurements by GC-MS and application to ^{13}C-metabolic flux analysis of the tricarboxylic acid cycle in *Brassica napus* leaves

Younès Dellero[1, 2, 4*], Solenne Berardocco[1, 2], Cécilia Berges[3, 4], Olivier Filangi[1, 2, 4], Alain Bouchereau[1, 2, 4]

[1]Institute for Genetics, Environment and Plant Protection (IGEPP), National Research Institute for Agriculture, Food and Environment (INRAE), Université Rennes, Institut Agro , Le Rheu, France

[2]Metabolic profiling and metabolomics platform, Institute for Genetics, Environment and Plant Protection, Biopolymers Interactions Assemblies, French National Research, Le Rheu, France

[3]TBI, Université de Toulouse, National center for Scientific Research (CNRS), National Institute for Research for Agriculture, food and Environment (INRAE), National Institute of Applied Sciences (INSA), Toulouse, France;

[4]MetaToul-MetaboHUB, National infrastructure of metabolomics and fluxomics, Toulouse, France

*** Correspondence:**
Corresponding Author
younes.dellero@inrae.fr

Keywords: Isotope, gas chromatography-mass spectrometry, trimethylsilyl (TMS) derivatives, accuracy, regulation, phosphoenolpyruvate carboxylase, decarboxylation, TCA cycle. (Min.5-Max. 8)

Abstract

The estimation of metabolic fluxes in photosynthetic organisms represents an important challenge that has gained interest over the last decade with the development of ^{13}C-Metabolic Flux Analysis at isotopically non-stationary steady-state. This approach requires a high level of accuracy for the measurement of Carbon Isotopologue Distribution in plant metabolites, which has still not been accurately evaluated at the isotopologue level for GC-MS. Thus, uncertainties remain about the accuracy of the CID measured and subsequently, the metabolic fluxes associated. Here, we developed a workflow to validate the measurements of CIDs from plant metabolites with GC-MS by producing tailor-made *E. coli* standard extracts harboring a predictable binomial CID for some organic and amino acids. Overall, most of our TMS-derivatives mass fragments were validated with these standards and at natural isotope abundance in plant matrices. Then, we applied this validated MS method to investigate the light/dark regulation of plant TCA cycle by incorporating U-^{13}C-pyruvate to *Brassica napus* leaf discs. We took advantage of pathway-specific isotopologues/isotopomers to show that the TCA cycle can operate in a cyclic manner at high rates in *Brassica napus* under both light and dark conditions. Notably, this forward cyclic flux mode has a nearly four-fold higher contribution to Citrate and Malate production than phosphoenolpyruvate carboxylase (PEPc) in our experimental setup. The light condition did not introduce an isotopic dilution to the dynamic of ^{13}C-enrichment in Citrate, Glutamate and Succinate compared to dark conditions and there was no evidence for significant variations of citrate pools in either light or dark conditions. Our results suggested that the contribution of stored citrate to the TCA cycle activity was unlikely to occur in *Brassica napus*. Interestingly, there was a light-dependent ^{13}C-incorporation into Glycine and Serine which revealed that TCA cycle-

derived CO_2 was actively reassimilated and contributed by up to 5% to net photosynthesis. We also observed an increase of PEPc contribution to malate production in the light while there was a higher involvement of PEPc-derived carbons to citrate production in dark condition. This suggested an important role for Malate import into mitochondria in sustaining TCA cycle in dark conditions.

1 INTRODUCTION

Metabolic fluxes within central metabolism are among the most important determinants of plant cell physiology, supporting central energetical functions and allowing them to quickly adapt to environmental changes by controlling metabolite turnover (Clark et al., 2020). Given that most of fluxes supported by a metabolic network cannot be measured directly, Metabolic Flux Analysis (MFA) technics were developed to infer information about metabolic fluxes from isotopic labeling experiments (Ratcliffe and Shachar-Hill, 2006).^{13}C-MFA relies on the tracing of ^{13}C throughout a metabolic network in a relative metabolic steady-state to model and/or compare metabolic fluxes, *i.e.* that the metabolic fluxes are stable across the experiment because the associated metabolite pool sizes are relatively constant over the time of labeling except for source (consumption) and sink (production) metabolites (Allen and Young, 2019;Antoniewicz, 2021). ^{13}C-MFA is usually performed at isotopic steady-state for heterotrophic tissues for practical reasons, and also because they can reach this isotopic state (Hay et al., 2014). Conversely, ^{13}C-MFA in phototrophic tissues can only be performed at isotopically non-stationary steady-state (INST-MFA), thus requiring a higher accuracy in the measurement of ^{13}C enrichment within metabolites (Cheah and Young, 2018). Over the last decades, ^{13}C-MFA has been applied successfully to microorganisms to highlight new metabolic routes and identify metabolic bottlenecks for the purpose of metabolic engineering (Cheah et al., 2020;Antoniewicz, 2021;Treves et al., 2022). In plants, ^{13}C-INST-MFA has been scarcely applied to date, due to the complexity in modelling accurately metabolic fluxes in a multicompartmental system (Heise et al., 2015;Kruger and Ratcliffe, 2021;Wieloch, 2021). However, accurate measurement of ^{13}C-enrichment is a prerequisite for precise evaluation of isotopic labeling dynamics and accurate modelling of metabolic fluxes. Indeed, small errors in mass isotopologue distribution can propagate to large errors in estimated fluxes (Antoniewicz et al., 2006).

Two major analytical methods are currently employed to analyze the Carbon Isotope Distribution (CID) within plant metabolites during ^{13}C-isotope tracing experiments: Nuclear Magnetic Resonance (NMR) and Mass Spectrometry (MS). NMR analysis of the ^{13}C enrichment is generally performed with ^{13}C-decoupling ^{1}H sequences and provides information at isotopomer level (by integrating ^{13}C-^{13}C interactions) (Kruger et al., 2007;Masakapalli et al., 2010;Abadie et al., 2017). Although this method is quantitative for the ^{13}C and allows to significantly separate carbon atoms of different chemical structures, it has a low sensitivity at natural ^{13}C abundance (large amounts of fresh material required), thereby affecting the accuracy for ^{13}C enrichment measurements regarding metabolites found in small quantities (Dellero et al., 2016;Abadie and Tcherkez, 2021). This method is also time-consuming due to the longer relaxation time for ^{13}C nucleus and the need to accumulate many spectrums to get a good signal (Abadie and Tcherkez, 2021). As a consequence, most of the ^{13}C-tracing isotope experiments recently performed in plants and analyzed by ^{13}C-NMR have only one time-point (Abadie et al., 2016;Abadie et al., 2018;Abadie and Tcherkez, 2019a;b), which questions the estimation of metabolic fluxes therein (metabolic/isotopic steady-state and treatment of metabolically inactive pools). To date, the accurate estimation of metabolic fluxes in phototrophic tissues requires to determine the isotopic and metabolic state of the system by coupling transient kinetics of ^{13}C-labeling with absolute quantification of metabolite pools (Kruger and Ratcliffe, 2015;Cheah and Young, 2018;Clark et al., 2020;Antoniewicz, 2021). Some methodological improvements were recently made with highly sensitive ^{1}H-derived sequences to improve the resolution of the ^{13}C atoms at the isotopomer

level (Sinnaeve et al., 2018), and its future use for ^{13}C-INST-MFA in plants will provide interesting perspectives. Conversely, mass spectrometry has been preferentially used to analyze the Carbon Isotope Distribution (CID) within plant metabolites during time-course ^{13}C-isotope tracing experiments (Szecowka et al., 2013;Ma et al., 2014;Medeiros et al., 2018;Treves et al., 2022). This method is more sensitive at natural ^{13}C abundance and can be implemented at high throughput. However, MS essentially gives information at the isotopologue level since isotopomer approaches are extremely limited by the availability of multiple MS fragments to cover the complete set of all possible isotopomers. An absolute quantification of the metabolite content is also required in general to subsequently infer metabolic fluxes. In addition, the analysis of CID for amino acids by LC-MS revealed some biases and errors in the measurement of CID (Heuillet et al., 2018), thus highlighting the need to evaluate measurement accuracy with GC-MS fragments for subsequent use in ^{13}C-MFA of plants.

Among plant metabolites, organic and amino acids are major players for plant primary metabolism. They are actively involved in crucial physiological processes such as photorespiration, *de novo* nitrogen assimilation and mitochondrial respiration (Xu et al., 2012;Zhang and Fernie, 2018;Dellero, 2020;Timm, 2020). Most of the carbon backbones for amino acid biosynthesis come from organic acids of the tricarboxylic acid (TCA) cycle (Galili et al., 2016). The functioning and regulation of the plant TCA cycle has been described based on flux balance models (Sweetlove et al., 2010;Araujo et al., 2012;Cheung et al., 2014) but also based on ^{13}C-labeling studies with different cells/experimental setups: attached leaves (Xu et al., 2021), detached leaves (Tcherkez et al., 2009;Gauthier et al., 2010;Zhang et al., 2021), leaf discs (Le et al., 2021), guard cell cultures (Daloso et al., 2017), heterotrophic cell cultures (Masakapalli et al., 2010). Overall, most of these works proposed that the plant TCA cycle is not cyclic in the light, with two branches acting separately: i) a first branch stimulated by the anaplerotic activity of phosphoenolpyruvate carboxylase (PEPc) leading to the production of Oxaloacetate, malate and fumarate; ii) a second branch stimulated by the entry of Citrate leading to the production of isocitrate, 2-oxoglutarate, glutamate and sometimes succinate. These conclusions were notably supported by the inhibition of the pyruvate dehydrogenase (PDH) complex and the mitochondrial respiration in the light while nitrogen assimilation was relatively high compared to dark conditions and required important amounts of 2-oxoglutarate (Tcherkez et al., 2005;Gauthier et al., 2010). However, the requirement to support continued export of sugar and amino acids from the leaf during the night and to meet cellular maintenance costs was also invoked (Cheung et al., 2014). Regarding the metabolic origin of citrate for the second branch in the light, it can come from: i) TCA cycle *de novo* biosynthesis using Acetyl-CoA derived from either glycolysis and alanine transamination; ii) a stored citrate pool in a light/dark dependent-manner; iii) the peroxisomal glyoxylate cycle (Gauthier et al., 2010;Sweetlove et al., 2010;Cheung et al., 2014;Dong et al., 2018;Le et al., 2021). Based on the NMR analysis of combined $^{13}CO_2$ and $^{15}NH_4{}^{15}NO_3$ labeling experiments in *Brassica napus* leaves, it was proposed that a high proportion of non-labeled citrate (vacuolar pool probably) was involved in the synthesis of 2-oxoglutarate under light conditions to sustain *de novo* nitrogen assimilation through glutamate (Gauthier et al., 2010). Under this scenario, the citrate pool would be replenished during dark conditions from glycolysis-derived ^{13}C-pyruvate, leading to a higher ^{13}C enrichment of the citrate after a light/dark cycle. Thus, the light and dark environmental conditions are expected to introduce important variations of metabolic fluxes within the plant TCA cycle (cyclic versus non-cyclic) and its associated PEPc anaplerotic pathway. Nevertheless, these variations remain to be carefully investigated in *B. napus* leaves with a ^{13}C-MFA framework, *i.e.* with time-course ^{13}C-isotope tracing experiments and pool size quantification.

Currently, the routine analysis of CID on plants is often assessed for organic and amino acids by GC-MS using TMS-derivatives (Szecowka et al., 2013;Araujo et al., 2014;Lima et al., 2018;Treves et al.,

2022). This TMS-based method notably allowed to follow the fate of sucrose breakdown within guard cells in connection with the TCA cycle (Medeiros et al., 2018). More recently, a ^{13}C-positionnal isotopomer approach was also proposed for glutamate and malate to investigate the fate of PEPc-derived carbon from ^{13}C-labeling experiments (Lima et al., 2021). Previous comparisons of two derivatization methods for GC-MS suggested that TBDMS-derivatives were potentially less prone to errors for amino acid analysis than TMS-derivatives (Antoniewicz et al., 2007;Young et al., 2014). However, the suitability of molecular ions from TMS and TBDMS derivatives was only performed using U-^{13}C-metabolites in each of these studies, which did not evaluate the entire CID but only the carbon distribution between the unlabeled isotopologue and the fully labeled isotopologue (M0 and M5 for a 5-carbon metabolite for example). Unfortunately, isotopic effects can occur at all stages of the analytical procedures and depend on the tested metabolite and its isotopic content. For instance, the present methodologies used have not assessed the impact of each isotopologue to the final isotopologue distribution, which can lead to important biases during the interpretation of the results. Thus, the reliability of CID measurements by GC-MS has to be evaluated for each individual isotopologue of all the compounds of interest to subsequently ensure a reliable use for monitoring isotopic labeling dynamics. This is even more important for plants, given that plant metabolites show strong differences of ^{13}C-enrichment dynamics between amino and organic acids (Szecowka et al., 2013). For this purpose, the recent development of an *E. coli* ^{13}C biological standard with controlled patterns of CID for organic and amino acids may help to address this issue (Millard et al., 2014). Indeed, the recent use of these reference samples allowed to identify important analytical biases in the CID measurement of Leucine and Asparagine in a concentration-dependent manner by LC-MS (Heuillet et al., 2018). Interestingly, this validated LC-MS method successfully measured nitrogen isotope distribution within plant amino acids and led to the accurate estimation of metabolic fluxes from ^{15}N-isotope transient labeling experiments in *B. napus* leaves at a metabolic steady-state using the ScalaFlux approach (Dellero et al., 2020b;Heuillet et al., 2020;Millard et al., 2020).

Here, we proposed a workflow to assess the measurement accuracy of CID from organic and amino acids by GC-MS for applications in plants. To do so, we built up an analytical method maximizing information on carbon backbones and analyzed two specific *E. coli* ^{13}C biological standards, produced to specifically harbor controlled patterns of CID for organic and amino acids (^{13}C-PT). We also analyzed chemical standards and plant samples at natural ^{13}C abundance to identify potential biases arising from matrix and analytical systems. Next, we applied our MS method to investigate the light/dark regulation of metabolic fluxes within plant TCA cycle by performing U-^{13}C-pyruvate labeling kinetic experiments on *B. napus* leaf discs under light or dark conditions. Using ^{13}C-MFA principles and some specific isotopologues, we calculated the fractional contribution of phosphoenolpyruvate carboxylase (PEPc) and TCA cycle to malate and citrate production and proposed a simplified carbon flux map with relative metabolic fluxes. Our results notably revealed that this TCA cycle/PEPc ratio was close to 4 for Malate and highlighted the cyclic nature of the TCA cycle in *B. napus* leaves. This ratio could be substantially regulated by light/dark conditions and mostly reflected the light-dependent activation of PEPc. In addition, we showed that pyruvate dehydrogenase and TCA cycle-derived CO_2 contributed to around 5% of net CO_2 assimilation under light conditions.

2 MATERIALS AND METHODS

Organisms and culture

The strain Escherichia coli K-12 MG1655 was grown on minimal medium containing 5 mM KH_2PO_4,10mM Na_2HPO_4, 9 mM NaCl, 40 mM NH_4Cl, 0.8 mM $MgSO_4$, 0.1 mM $CaCl_2$, 0.3 mM thiamine, and 45 mM of the ^{13}C-labeled Acetate mixture as the sole carbon source. Acetate and

thiamine were sterilized by filtration, whereas the other compounds were autoclaved separately. Batch cultures were carried out in 1-L baffled flasks with 500 mL of medium sparged with synthetic gas (80% N_2/20%O_2 containing <1 ppm CO_2, Air Liquide). Cultivation was performed in a Multifors Bioreactor (Infors HT, Bottmingen-Basel, Switzerland) at 37 °C and 200 rpm of orbital shaking. The pH was maintained at 7.0 by the addition of 2 M HCl. Cell growth was monitored by measuring optical density at 600 nm with a Genesys 6 spectrophotometer (Thermo, Carlsbad, CA, USA). Amount of biomass in each sample was calculated using a coefficient of 0.37 g of cell dry weight per OD unit. Arabidopsis thaliana seeds were sterilized for 10 min with absolute ethanol containing 7.5% NaClO and rinsed two times with absolute ethanol. Seeds were sowed on ½ MS media containing 1% Agar and incubated to the dark at 4°C for 48-72 hours to break seed dormancy. Seedlings were grown at ambient air under a day/night cycle with 16 h light/8h dark at a light intensity of 120 µmol photons.m^{-2}.s^{-1} and 20°C day/18°C night. Seedlings were harvested after 2-3 weeks by instant sampling with liquid nitrogen and lyophilized for 96 h before to be stored at -80°C until analysis. Two-month old *Brassica napus* plants were obtained from seeds exactly as described before (Dellero et al., 2020a). The leaf L9 was used for all experiments (natural ^{13}C abundance and U-^{13}C-pyruvate incorporation).

U-^{13}C-pyruvate labeling experiments

Four hours after the beginning of the light period, each leaf was cut at the basis of the petiole and then 66 leaf discs (0.8 cm^2) were randomly punched with a cork-borer in both laminas of each leaf. Leaf discs were first floated in a 10 mM MES-KOH (pH 6.5) buffer for 15 min in order to process the L9 leaf for four plants (see details for leaf annotation in (Dellero et al., 2020a)). In this experiment, one leaf of a plant corresponded to a biological replicate. Then for each time point, six leaf discs from the same leaf were transferred in a well of a 6-well microplate filled with 4 mL/well of a buffer containing 10 mM MES-KOH (pH 6.5) and 10 mM U-^{13}C-Pyruvate (^{13}C isotopic purity of 99%; sodium salt from Cambridge Isotope Laboratories (Eurisotop, France)). All incubations were performed at 20 °C with an orbital shaking of 70 rpm under either a continuous light of 120 µmol photons m^{-2} s^{-1} or under dark conditions using multiple opaque plastic bags, similarly to the previous experimental set-up used for dark-induced senescence (Dellero et al., 2020a). The timepoint 0 was the same for both conditions as it corresponded the beginning of the experiment. For each time point (0, 0.5, 1, 2, 4, 6 hours of incubation), the leaf discs were harvested and rinsed three times (10 sec) with a neutral buffer (i.e., without U-^{13}C-Pyruvate) and dried for 10 s on a clean tissue before being frozen in liquid nitrogen and stored at -80 ◦C. The timepoint 0 of the experiment was incubated 2 sec with the labeled buffer before being rinsed in order to evaluate the fraction of $^{13}C_3$-pyruvate detected in our analysis that was not incorporated inside leaf discs (leading to a mean ^{13}C enrichment close to 35% for pyruvate at T0 in our study).

Analysis of ^{13}C-labeled Acetate by NMR

An equimolar mixture of all ^{13}C-isotopomers of acetate was produced from ^{12}C-Acetate, 1-^{13}C-Acetate, 2-^{13}C-Acetate and U-^{13}C-Acetate (^{13}C isotopic purity of 99%, sodium salts from Cambridge Isotope Laboratories (Eurisotop, France); **Figure 1**). Quantitative 1H 1D- NMR was used to control the isotopic composition of the ^{13}C-labeled substrate before use. NMR spectra were recorded with an Avance 500 MHz spectrometer (Bruker, Rheinstetten, Germany) at 298 K, using a 30° pulse and a relaxation delay of 20 s. The proportion of each isotopic form was quantified by fitting using a mixed Gaussian−Lorentzian model (Millard et al., 2017).

Metabolite extraction and quantification

^{13}C-PT full metabolites and ^{13}C-PT protein hydrolysates extracts were obtained following procedures described previously (Heuillet et al., 2018). Briefly, for the ^{13}C-PT full metabolites extract, 1 mL of *E. coli* broth at OD600 nm = 1.7 was micro-filtered and the pellet was rapidly quenched at -20 °C into a mixture of acetonitrile/methanol/H_20 (2:2:1) with 0.1% formic acid. After a centrifugation step (7000g, −20 °C, 15 min), the supernatant was evaporated and resuspended in 250 µL of Milli-Q water, to be stored at −80 °C until analysis. For the ^{13}C-PT protein hydrolysates extract, the pellet obtained with the cellular extract was subjected to an acid hydrolysis with 6N HCl at 110 °C overnight. Samples were evaporated and rinsed 3 times with Milli-Q water. After a centrifugation step (10 min, 12 000g), the supernatant was stored at −80 °C. Polar metabolites of freeze-dried Arabidopsis seedlings and *B. napus* leaves were extracted with a MeOH/Chloroform/H_2O mixture following procedures described previously (Dellero et al., 2020b). The quantification of amino acid content was performed by HPLC-UV exactly as described previously (Dellero et al., 2020b). The quantification of organic acids was performed by GC-FID exactly as described previously (Bianchetti et al., 2021).

Determination of Carbon Isotopologue Distribution by GC-MS

Dried aliquots of samples were derivatized on a MultiPurpose Sampler Gerstel and analyzed by GC-MS (GC-2010 Plus Shimadzu coupled to a triple quadrupole mass spectrometer GCMS-TQ8040 Shimadzu). Polar metabolites were first derivatized for 1 h at 40°C with 50 µL of pyridine containing 20 g.l^{-1} methoxyamine chloride and then were incubated with 50 µL of N-Methyl-N-(trimethylsilyl)-trifluoroacetamide (MSTFA) for 0.5 h at 40°C. 1 µL was injected with a split mode 1/20 at 260°C on a TG-5MS column (26098-1420, Thermo Scientific). Separation was performed in a Helium gas-stream at 1 mL.min^{-1} using the following temperature ramp : 4 min at 70°C, +10°C.min^{-1} until 198°C, 2 min at 198°C, +1°C.min^{-1} until 202°C, +15°C.min^{-1} until 268°C, 3 min at 268°C, +1°C.min^{-1} until 272°C,+10°C.min^{-1} until 310°C and 7 min à 310°C. The transfer line was maintained at 300°C and the ion source at 200°C. Ionization was performed by electron impact at 70 eV and the MS acquisition was carried out after a solvent delay of 5 min in full scan mode at 7 spectra.s$_{-1}$ over the m/z range 45-700. MS Spectra were processed with the software "GCMS Solutions" supplied by Shimadzu to adjust retention times between each run using a mixture of alkanes (C7 to C40, Sigma-Aldrich). Peak identity was established according to their retention time and mass fragmentation spectra with respect to authentic standards derivatized (**Table S1**), and by reference to mass spectra of derivatives in the US National Institute of Standards and Technology database and in the Golm metabolome database. All mass isotopologue raw areas were subjected to correction for the contribution of naturally occurring isotopes of all elements except the carbon arising from the metabolite backbone using the IsoCor v2.1.4 package of Python (https://github.com/MetaSys-LISBP/IsoCor) in low resolution mode (Millard et al., 2019). In addition, unlabeled chemical standards and Arabidopsis and *B. napus* leaves were additionally corrected for the contribution of naturally occurring isotopes of the carbon arising from the metabolite backbone (giving a residual molecular ^{13}C enrichment of 0 for molecules labeled at natural ^{13}C abundance). ^{13}C-PT samples were not concerned by this additional correction since they held fully controlled ^{12}C/^{13}C patterns at all positions. A correction method dedicated to IsoCor was specifically created for the TMS-derivative fragment described in this study (**Table 1**), *i.e.* by considering the contribution of all atoms added by the derivatization on the isotopic measurement of the monitored fragments (chemical separation of all atoms arising from the metabolite and the derivative). All files required to run this method on IsoCor are available in the supplementary material of this article (**Supplementary files**) and all information will be updated indefinitely in the following INRAE dataverse (Dellero and Filangi, 2021). The method is publicly available and can also be run directly from GC-MS source files using the following Galaxy workflow (https://galaxy.genouest.org/, section "Metabolomics", subsections "Conversion GCMS PostRun Analysis to IsoCor" and "Isotope Correction for mass spectrometry labeling experiments"). For this purpose, each raw GC-MS dataset

should contain a column "Name" for the fragments considered and a column "Area". The name of each fragment must be written exactly as specified in the "Metabolite.dat" (an example file is provided in the **supplementary material**). Fractional Carbon Isotopologue Distribution and mean ^{13}C enrichment were directly obtained from IsoCor outputs (isotopologue_fraction and mean_enrichment) while CIDs were converted to binomial distributions by multiplying with 2^n, where n is the number of carbon atoms (Millard et al., 2014). The accuracy of measurements was assessed from the closeness of experimental and predicted values for CIDs and mean ^{13}C enrichments at either ^{13}C-PT abundance or at natural ^{13}C abundance. CID accuracy was formally defined as the mean of absolute differences between measured and predicted values for each isotopologue (Heuillet et al., 2018).

Pathway fractional contribution

Pathway fractional contribution (FC) can be applied to a metabolic network in a metabolic and isotopic steady-state to compare the relative contribution of the considered pathway to the production of a metabolite, as long as these pathways produced specific isotopologues that can be monitored (Buescher et al., 2015). Here, FC was calculated from PEPc and TCA cycle-specific mass isotopomers/isotopologues for Malate and Citrate from the timepoint 4 and 6 hours (metabolic steady-state and pseudo-isotopic steady-state for isotopologue ratios). In the following equations, *mi* refers to the isotopologue enrichment calculated with respect to the CID (sum of all *mi* for a given metabolite equal to 1). As all these calculations are relative, it is also possible to use corrected areas of mass isotopologues (outputs from IsoCor). For Malate_3TMS_C1C4 (corresponding to the GC-MS fragment from Malate(3TMS) metabolite than contained the C1-C2-C3-C4 carbons of Malate (**Table1**)), M1 isotopologue measurement reflected both PEPc and TCA cycle isotopomers (**Figure 6**). However, the ratio between M1 and M3 isotopologues of Malate_3TMS_C1C4 produced by the TCA cycle (denoted *X* in the following equations) can also be observed in Succinate_2TMS_C1C4 and Glutamate_2TMS_C2C5, thereby reflecting the M0 and M2 from mitochondrial active pool of Acetyl-CoA, *i.e.*:

$$SuccinateC1C4\left(\frac{m3}{m1+m3}\right) = GlutamateC2C5\left(\frac{m3}{m1+m3}\right) = Acetate\left(\frac{m2}{m0+m2}\right) = X$$

From this parameter, we calculated the FC of PEPc and TCA cycle to Malate and Citrate production as follows:

$$FC\ Malate_{PEPc} = MalateC1C4\left(\frac{m1-\left(\left(\frac{1-X}{X}\right)\times m3\right)}{m1+m2+m3}\right)$$

$$FC\ Malate_{TCA\ cycle} = MalateC1C4\left(\frac{m2+\frac{m3}{X}}{m1+m2+m3}\right)$$

$$FC\ Citrate_{PEPc} = CitrateC1C6\left(\frac{m1+m3}{m1+m2+2\times m3+m4}\right)$$

$$FC\ Citrate_{TCA\ cycle} = CitrateC1C6\left(\frac{m2+m3+m4}{m1+m2+2\times m3+m4}\right)$$

It should be noted that *m3* was used twice in the FC Citrate calculations because this isotopologue is produced by both pathways. Finally, the FC of pyruvate dehydrogenase (PDH) and TCA cycle-derived CO_2 to photosynthesis was calculated using *X* as a proxy for the $^{13}C/^{12}C$ ratio of this CO_2 fraction in light conditions. Considering the isotopic and metabolic steady-state for these metabolites, the mean ^{13}C enrichment of *X* should be observed in Serine if this fraction of CO_2 accounted for 100% of CO_2 fixed by photosynthesis, *i.e.:*

$$FC\ photosynthesis_{PDH\ and\ TCA\ cycle\ CO_2} = \frac{mean\ ^{13}C\ enrichment\ (SerineC1C3)}{X}$$

Mean ^{13}C enrichment of Serine C1C3 was recalculated from M1 isotopologue of Serine_2TMS_C1C2 and Serine_2TMS_C2C3 assuming that Serine was only labeled in the C2 of these fragments based on the validated hypothesis (**Figure 7B**).

Statistical analysis

Statistical comparisons were performed using either confidence intervals (comparison of a group of value against one reference value), a Student-test (comparison of 2 groups of values) or an ANOVA followed by a post-hoc Tukey-HSD test (comparison of 3 or more groups of values) with a level of p-value <0.05 by using the publicly available Rstudio software (RStudio Team, 2016).

3 RESULTS

The proposed workflow (**Figure 1**) consisted in three steps: 1) the build-up of a method to identify and select abundant molecular ions deriving from TMS-derivatives with a large number of carbons; 2) the production of two reference ^{13}C-labeled samples with a controlled pattern for CID (^{13}C-PT) using *E. coli* as a metabolic factory; 3) the validation of TMS-derivatives mass fragments for CID measurements with our GC-MS method for applications in plants using ^{13}C-PT reference samples and unlabeled and ^{13}C-labeled plant samples.

Selection of GC-MS mass fragments maximizing information on carbon back-bones of organic and amino acids

We combined a literature survey analyzing common pathway of TMS-derivative mass fragmentations with the injection of chemical standards in our analytical system to select some abundant fragments maximizing the information on carbon backbones. Their chemical identity was further confirmed by the observed CID pattern with our two reference ^{13}C-PT samples. Derivatives with only one TMS group were not considered in this study due to the low yield of these fragments after fragmentation and the occurrence of important contaminations for low m/z. Overall, TMS-derivatives of most α-amino acids were characterized by an α-cleavage of the carboxylic function in the form of a TMS-CO_2 (m/z 117) (Harvey and Vouros, 2020), thus leading to the abundant formation of fragments containing all others atoms of the α-amino acids except the C1 (**Table 1**). Only Ornithine(4TMS) could be detected without any mass loss (**Table 1**, (Harvey and Vouros, 2020)). Aromatic amino acids showed an additional α-cleavage of the amine function leading to the additional production of an abundant m/z 218 fragment containing the C1-C2 for Phenylalanine, Tryptophan and Tyrosine (**Table 1**, (Lai and Fiehn, 2018;Harvey and Vouros, 2020)). Only tryptophan did not proceed through an α-cleavage of the carboxylic function compared to Phenylalanine and Tyrosine, but the other fragment containing the C3 to C11 atoms resulting from the α-cleavage of the amine function could be abundantly detected. Serine(3TMS) and Valine(2TMS) showed also some specific abundant molecular ions in addition to the α-cleavage of the carboxylic function (**Table 1**,(Harvey and Vouros, 2020)). Arginine, Histidine

and Cysteine could not be detected by GC-MS using TMS derivatization and were not further considered in our study. Beside this, β-Alanine, an important β -amino acid from plants, showed a classical abundant fragment resulting from the loss of methyl from a TMS group, which is known to be very low in α-amino acids (**Table 1**, (Lai and Fiehn, 2018)). Interestingly, fragmentation of the TMS-derivatives of organic acids related to the TriCarboxylic Acid cycle proceeded through an α-cleavage within a TMS group leading to the loss of a methyl radical and producing a [M-15] fragment containing all carbon atoms. However, this fragment was very weak for Citrate and Malate. The highest fragments maximizing information on carbon backbones were m/z 273 (C1 to C5) for Citrate(4TMS) and m/z 233 (C2 to C4) for Malate(3TMS). The identity of the carbons hold by these fragments has been recently assigned using position-specific ^{13}C-labeled standards prepared by *in vitro* enzymatic reactions (Okahashi et al., 2019).

Evaluation of CID measurements by GC-MS using reference ^{13}C-PT samples and plant samples at natural isotope abundance

Next, we produced reference ^{13}C-labeled samples using *E. coli*, denoted here ^{13}C-PT. This strategy relies on the use of an accurate equimolar mixture of all ^{13}C isotopomers of acetate to biologically produce metabolites with fully controlled and predictable ^{13}C-labeling patterns (Millard et al., 2014). Thus, molecular ^{13}C enrichment of each carbon-containing metabolite will be theoretically equal to 50% and all isotopomers will be present in equimolar concentrations, leading to a binomial distribution of isotopologues following Pascal's triangle. For this purpose, we grew *E. coli* in a minimal media with this acetate mixture as the sole carbon source of the media (**Figure 1**) and checked its isotopic content by NMR (molecular ^{13}C enrichment expected at 49.9 % ± 0.8). From cell harvest, two specific reference ^{13}C-PT samples were produced during the extraction: i) a ^{13}C-PT full metabolite extract containing all polar metabolites for the evaluation of CID for organic acids; ii) a ^{13}C-PT protein hydrolysates extract containing proteogenic amino acids in high concentrations for the evaluation of CID for amino acids. This strategy allowed to maximize the amount of amino acids that can be weakly abundant as soluble pools when *E. coli* is grown in a minimal media. It should be mentioned that the hydrolysis process deamidated Asparagine into Aspartate and Glutamine into Glutamate, thus these amino acids could not be evaluated (Kambhampati et al., 2019). In addition, non-proteogenic amino acids from the **Table 1** could not be evaluated with this extract (Ornithine, β-Alanine).

To facilitate comparison of CIDs between the different amino acids, we converted the measured ^{13}C-enrichments among isotopologues of each fragment into binomial distribution, thus reflecting the number of isotopomers considered for each isotopologue (**Figure 2** and Material and Methods). In the following figures, GC-MS fragments will be denoted according to the considered metabolite, its TMS-derivative analyzed and the metabolite carbon backbone (for example, Glutamate_3TMS_C2C5 means that the fragment contains the carbon C2-C3-C4-C5 (**Table1**)). Overall, all the considered amino acids were detected in the ^{13}C-PT protein hydrolysates except Tryptophan (**Figures 2A, S1A**). We found very a high level of correlation between the measured CID (blue bars) and the expected CID (black bars) for numerous amino acid fragments considered in our method: α-Alanine_2TMS_C2C3, Aspartate_C2C4 either in 2TMS or 3TMS, Glutamate_3TMS_C2C5, Glycine_3TMS_C2, Isoleucine_2TMS_C2C6, Leucine_2TMS_C2C6, Phenylalanine_2TMS_C1C2 and C2C9, Serine_2TMS_C2C3, Serine_3TMS_C1C2 and C2C3 and Tyrosine_2TMS_C1C2. CID measurements for Methionine_2TMS_C2C5 showed a high variability coupled to a lower estimation of M3 and M4 isotopologues at the expense of M1 and M2 (**Figure 2A**). However, this amino acid was in a very low abundance in the ^{13}C-PT protein hydrolysates compared to the others amino acids (**Figure S1A**). Lysine and Tyrosine_2TMS_C2C9 had also important variability for their CID measurements, leading to misestimations of their M3 isotopologues. The most important and

significant errors for CID measurements of amino acids concerned Proline_2TMS (overestimation of M4), Threonine_3TMS (overestimation of M3 at the expense of M0 and M1), Valine_2TMS_C1C2 (overestimation of M2) and Valine_2TMS_C2C5 (overestimation of M3 at the expense of M1 and M2). Considering the recent establishment of a ^{13}C-positional isotopomer approach for Glutamate to analysis its C1 carbon (Lima et al., 2021), we also analyzed the CID for the two low abundant fragments Glutamate_3TMS_C1 (CO_2-TMS, M0 at m/z 117) and Glutamate_3TMS_C1C5 fragment (CH3 loss, M0 at m/z 348). However, they both showed large and significant misestimations of their CIDs, thus questioning the accuracy of this isotopomer-based method (**Figure S1B**). The analysis of organic acids from ^{13}C-PT full metabolites extract showed relatively good CID for Citrate_2TMS_C1C5, Malate_3TMS_C2C4 and Fumarate_2TMS_C1C4 (**Figure 2B**). Citrate_4TMS_C1C6 and Malate_3TMS_C1C4 showed also relatively good CID but they had a higher variability compared to their respective C1C5 and C2C4 fragments. There was a very high overestimation of M0 in Succinate_2TMS_C1C4, which seemed to have an impact on M2, M3 and M4 isotopologues, However, these misestimations for Succinate have been previously attributed to contaminations inherent in the ^{13}C-PT full metabolites extract used here (Millard et al., 2014), thus preventing the analytical validation for this fragment. For Pyruvate_MEOXTMS_C1C3, the variability was too high to assess the CID measurements, perhaps reflecting its weak derivatization yield and low abundance in ^{13}C-PT full metabolites extract (**Figure S1A**). To further assess the distribution of measurement errors among isotopologues, we analyzed the CID accuracy, using threshold values of ±0.05 (**Figure 3A**). Overall, the bias of measurement for each isotopologue of each metabolite was relatively low except for Methionine, Valine, Threonine, Succinate and Pyruvate. Interestingly, these very high levels of accuracy for CID measurements were converted into very high levels of accuracy for mean ^{13}C enrichment measurements, leading to very small shifts between expected (0.499 ±0.08) and measured values (below 1% of error), except for Methionine, Valine, Threonine, Succinate and Pyruvate (**Figure 3B**). However, Malate_3TMS_C1C4, Lysine_2TMS_C2C6 and Serine_2TMS_C2C3 showed important variability for mean ^{13}C enrichment measurements although no strong biases in their CID measurements were previously observed. Conversely, mean ^{13}C enrichment of Phenylalanine_2TMS_C1C2 and proline_2TMS_C2C5 were slightly overestimated and reflected the overestimation of their respective isotopologues M2 and M4. To ensure that the tested fragments were suitable for isotopic analyses of metabolites from plant samples, we analyzed their accuracy at natural ^{13}C abundance. For this purpose, we produced two types of plant samples (seedlings from Arabidopsis and leaves from *B. napus*) and we measured the CID for each fragment of our method to calculate the residual molecular ^{13}C enrichment (**Figure 3C**).

This variable corresponded to the ^{13}C enrichment remaining after removing the contribution of natural abundance for all isotopes (a value of 0 is expected if no contamination occurs). Among the metabolites that were detected in the plant samples, most of the fragments for organic and amino acids showed relatively high accuracy at natural ^{13}C abundance, with most of the mean values of residual molecular ^{13}C enrichment ranging between and 0.05 and 3% (**Figure 3C**). Interestingly, some discrepancies were observed between Arabidopsis seedlings and *B. napus* leaves, notably for the full carbon backbone fragments Citrate_4TMS_C1C6 and Malate_3TMS_C1C4, which were more accurately measured in *B. napus* at low enrichment levels (critical values close to 5% for Arabidopsis). Conversely, Arabidopsis seedlings showed slightly higher accuracies than *B. napus* leaves for AlphaAlanine_2TMS_C2C3, Aspartate_2TMS_C2C4, Fumarate_2TMS_C1C4 and Serine_3TMS fragments. Phenylalanine_2TMS fragments showed residual molecular ^{13}C enrichments close to 5% but only in plants samples. Surprisingly, Proline_2TMS_C2C5, Threonine_3TMS_C2C4 and Valine_2TMS_C2C5 showed relatively important residual molecular ^{13}C enrichments (nearly 10%) in both chemical standards and unlabeled plant extracts, suggesting the occurrence of analytical bias. A detailed survey showed that the isotopic cluster of Proline_2TMS_C2C5 was contaminated in the M4

isotopologue (m/z 146) by a mass fragment deriving from near elution of Isoleucine_2TMS, and correlated with previous measurements of CIDs (**Figures 2, 3D**). Similarly, the isotopic cluster of Valine_2TMS_C2C5 was contaminated in the M3 isotopologue (m/z 147) while Threonine_3TMS_C2C4 showed a surprising very high abundance of the M1 isotopologue (40% of the CID) in both chemical standards and unlabeled plant extracts.

Assessment of the light/dark regulation of TCA cycle and PEPc fluxes in *Brassica napus* leaves using a ^{13}C-MFA approach

To further validate our MS method, we applied it to ^{13}C-labeled plant samples. For this purpose, we performed transient kinetics of U-^{13}C-pyruvate incorporation to *B. napus* leaf discs subjected to either light or dark conditions for up to 6 hours. The aim of this experiment was to obtain an overview of the light/dark regulation of metabolic fluxes associated to TCA cycle and PEPc using MS methodology and isotopologue-based approaches. We used U-^{13}C-pyruvate as a probe since the mitochondrial Pyruvate DeHydrogenase (PDH) will be able to produce simultaneously $^{13}C_2$-Acetyl-CoA molecules suitable for the investigation of the TCA cycle and $^{13}CO_2$ molecules suitable for the investigation of PEPc activity through the combined action of carbonic anhydrase ($H^{13}CO_3^-$).

Following our experiments, the analysis of mean ^{13}C enrichment for all conditions revealed a significant increase for α-Alanine, Aspartate, Citrate, Glutamate, Glycine, Malate, Pyruvate, Serine and Succinate along the U-^{13}C-pyruvate incorporation (**Figure 4A**, **Table S2**; **Table S4** for statistical analysis). There was a very high biological variability and small ^{13}C enrichment for Fumarate_2TMS_C1C4. Overall, most of these enrichment dynamics remained relatively equivalent between light and dark conditions for all the fragments considered, except for Glycine and Serine, which were almost exclusively enriched in light conditions. These results were surprising since previous experiments using a 4-hour incorporation of 15 mM U-^{13}C-pyruvate into Arabidopsis leaves showed a higher mean ^{13}C enrichment for Citrate, Glutamate and succinate in the *pdk* mutant (light-dependent activator of the PDH complex) compared to the control (Zhang et al., 2021). Considering Glycine and Serine, the importance of the light-dependent photorespiratory pathway for their production in leaves clearly suggested that a significant part of $^{13}CO_2$ arising from PDH and TCA cycle decarboxylations (isocitrate dehydrogenase and 2-oxoglutarate dehydrogenase) was reassimilated by photosynthesis. A statistical analysis revealed that Glycine_3TMS_C2, Serine_3TMS_C1C2 and Serine_3TMS_C2C3 reached a pseudo-isotopic steady-state starting after 2 hours of illumination (**Table S4**). Other fragments showed a relatively linear evolution of their mean ^{13}C enrichment, except for Pyruvate_MEOXTMS_C1C3 which rapidly reached an isotopic steady-state after 0.5 hours only. Interestingly, labeling data from Pyruvate_MEOXTMS_C1C3 and Succinate_2TMS_C1C4 fragments had a very good resolution (weak analytical and biological variability) compared to previous evaluation with ^{13}C-PT full metabolites extract. Next, we performed quantification of metabolite pool sizes along the experiment to determine whether the considered metabolic network was in a metabolic steady-state (**Figure 4B, Table S3**). For this purpose, we used GC-FID for organic acids and UPLC-UV for amino acids using AccQTag methodology as they have a very high level of stability for absolute quantification. Indeed, TMS-derivatives of amino acids are highly unstable along a GC-MS run, leading to drastic differences of response when quantifying them with external standards curves (Data not shown). In addition, the reliable absolute quantification of metabolites using their CID masses can only be achieved by using internal isotopic standards for each metabolite considered (not our case in the present study) (Heuillet et al., 2020;Evers et al., 2021). Overall, metabolite pool sizes were relatively different for each of them but there was no significant difference between light and dark conditions, except for Aspartate. Glycine was only quantified in light conditions (not detected in “dark condition” samples with UPLC-UV). Interestingly, a statistical analysis showed that all the metabolite

pool sizes reached a significant pseudo steady-state starting after 1 hour (similar statistical groups in **Table S5**). To summarize, we have found some similar ^{13}C enrichment dynamics for TCA cycle derived metabolites in both light and dark conditions combined to similar metabolite pool sizes at a metabolic steady-state.

Next, we focused our analysis on the isotopologue dynamics of these metabolites in order to depict the considered metabolic network and compare metabolic fluxes associated to TCA cycle and PEPc (**Figure 5**). Mean ^{13}C enrichment of Citrate, Glutamate and Succinate was essentially driven by an increase of the M2 isotopologue for light and dark conditions, thus reflecting the incorporation of M2 Acetyl-CoA arising from U-^{13}C-pyruvate. However, there was also an increase of M1 and M3 isotopologues for Glutamate and Succinate after 2 hours while M1, M3 and M4 isotopologues of Citrate_4TMS_C1C6 and Citrate_2TMS_C1C5 were increased starting from 4 hours. M1 and M4 of Citrate_4TMS_C1C6 were essentially increased in dark conditions compared to light conditions after 4 hours. There was a very high variability for Fumarate_2TMS_C2C4 CID in both conditions, which prevented its use for a reliable isotopic investigation. Interestingly, Malate_3TMS_C1C4 fragment showed a higher enrichment of M1 compared to M2 in the light condition while M2 remains higher than M1 in the dark condition. This shift may reflect an increase of the PEPc activity under light condition (M1 arising from the reassimilation of the mitochondrial $^{13}CO_2$ decarboxylations). Since there was no difference of mean ^{13}C enrichment between light and dark conditions for this fragment (**Figure 4A**), this result reinforced the importance of analyzing specifically CIDs for the interpretation of labeling data. In addition, the CID of Malate_3TMS_C2C4 showed a similar dynamic for both light and dark conditions, hence ruling out the use of this fragment to disentangle PEPc and TCA cycle contribution to Malate production (**Figure 5**). Aspartate_3TMS_C2C4 showed a very high variability for the light condition, but the CID dynamic in the dark condition was similar to the CID dynamic of Malate_3TMS_C2C4. Thus, both fragments seemed to mimic Oxaloacetate labeling dynamics. Pyruvate_MEOXTMS_C1C3 was only enriched with the M3 isotopologue (nearly 80% M3/20% M0), thereby suggesting that the activity of the malic enzyme, converting malate to pyruvate, was negligible in our metabolic network.

From these observations, we built a simplified metabolic network for TCA cycle composed of two "turns" to explain the production of M1 and M3 in both Succinate_2TMS_C1C4 and Glutamate_2TMS_C2C5 (**Figure 6A**). In this network, the second "turn" reflected the commitment of a molecule that has already experienced all reactions of the TCA cycle to another round of reactions (Orange and blue labels to compare acetyl-CoA-derived labeling from 1st and 2nd "turn"). Based on previous works (Abadie and Tcherkez, 2019a), the reverse reaction of the fumarase was also considered in the network, although it has no effect on the M1 isotopologue monitored by mass spectrometry (C4 and C1 isotopomers are still detected as M1 isotopologues in our study). The involvement of a light-dependent stored ^{12}C-Citrate pool was not represented here since it only provided M0 isotopologues (no additional isotopologues to explain). From this metabolic network, we proposed to evaluate PEPc-dependent and TCA cycle-dependent contributions to Citrate production through M1, M2, M3 and M4 isotopologues and to Malate production through M1, M2 and M3 isotopologues. These contributions were only calculated using timepoints 4 and 6 hours, because all the fragments to consider for these contributions were mostly visible at these moments. The main idea of this pathway fractional contribution (FC) to a given metabolite production rely on the use of pathway-specific mass isotopomer ratios for the metabolite considered, as long as the metabolic network is in a metabolic and isotopic pseudo steady-state. Here, we observed a rapid metabolic steady-state (**Figure 4B**, **Table S5**) and a relatively negligible evolution of the ratios for the considered isotopologues between 4 and 6 hours (comparison of ratios for M1, M2 and M3 isotopologues only for Malate for example). In this context, the relative contribution of PEPc and TCA cycle to either Malate and Citrate production remained in

the same order of magnitude between T4 and T6 hours (**Figure 5**). An important issue to address for calculating FC concerned the M1 from Malate_3TMS_C1C4, which monitored at the same time PEPc and TCA cycle dependent isotopomers. To deal with, we took advantage of Succinate_2TMS_C1C4 and Glutamate_2TMS_C1C4 fragments which both harbored M1 and M3 isotopologues that are the precursor of TCA cycle-dependent M1 and M3 of Malate_3TMS_C1C4 (**Figure 5**). Analysis of the M1/(M1+M3) ratio for these two fragments showed a remarkable stability between dark and light conditions, thus reflecting a stable M2 enrichment of 40% for the active pool of acetyl-CoA (**Figure 6 B** and Equations). This result also showed that the isotopologue ratios considered here were at a pseudo isotopic steady-state. Using this ratio, we calculated the FC of PEPc and TCA cycle for malate and citrate respectively (**See equations**). We found that TCA cycle had a significant four-fold higher contribution to either Malate or Citrate production compared to PEPc in all conditions (around 80% versus 20%). Interestingly, there was a 1.6-fold increase of the FC of PEPc to Malate production from dark to light conditions (14% versus 23%), although it remained not statistically significant (high variability, t-test p-value =0.08). Conversely, PEPc contribution to Citrate production was significantly 1.5-fold higher in dark condition than in light condition (26% versus 17%). Thus, the results suggested a higher commitment of PEPc-derived carbons to the forward part of the TCA cycle in the dark, while commitment of PEPc-derived carbons to the reverse part of the TCA cycle (Malate and perhaps Fumarate) was reduced at the same time.

Finally, we explored the isotopologue distribution of Glycine and Serine, some amino acids which were previously identified as a proxy for photosynthetic reassimilation of PDH and TCA cycle-derived $^{13}CO_2$ (**Figure 7A**). Our results showed that the increase of mean ^{13}C enrichment for the three considered fragments in light condition came from an increase of their M1 isotopologue. Given that the light-dependent photorespiratory enzymes glycine decarboxylase and serine:hydroxymethyl aminotransferase convert 2 glycine into 1 serine, we wanted to know whether the fragments Serine_2TMS_C1C2 and Serine_2TMS_C2C3 were labeled in the same or different carbons, thus revealing if the C1 of Glycine was also labeled (**Figure 7B**). By reviewing all the possible scenarios with different combinations of labeled glycine, we showed that the CID associated to our fragments (isotopologue occurrence) could only be produced with one molecule of glycine labeled at the C2 and an unlabeled molecule of glycine, leading to the production of a molecule of Serine labeled only at the C2 and an unlabeled CO_2 molecule. Since we have shown that Glycine and Serine were both at the isotopic and metabolic steady-state between 2 and 6 hours (**Figure 4**, **Table S4**, **Table S5**), we used Serine fragments to evaluate the contribution of PDH and TCA cycle-derived CO_2 to the photosynthetic activity. For this purpose, the steady-state enrichment of Acetyl-CoA calculated before was used as a proxy of the $^{12}C/^{13}C$ ratio of the CO_2 produced by pyruvate dehydrogenase since a significant proportion of PDH-derived ^{12}C could still contribute to photosynthesis (**See equations**), and given its presumable contribution for light respiration (CO_2 emissions) (Tcherkez et al., 2005). After recalculating the mean ^{13}C-enrichment of SerineC1C3 from both Serine fragments (C1-C2 or C2-C3), we showed that the light-dependent assimilation of PDH and TCA cycle decarboxylations could represent around 5% of net photosynthesis (**Figure 7C**).

4 DISCUSSION

The estimation of metabolic fluxes in photosynthetic organisms represents an important challenge that has gained interest over the last decade with the development of ^{13}C-INST-MFA. This approach requires a high level of accuracy for CID measurements to avoid propagation of small measurement errors to large errors in estimated fluxes (Antoniewicz et al., 2006). Considering the need to perform high throughput measurements at isotopically non-stationary steady-state, MS has been preferentially selected by the field in the recent years to measure CID in organic and amino acids. However, the

suitability of TMS-derivative molecular ions for these metabolites has never been evaluated at the isotopologue level, *i.e.* by monitoring the impact of each isotopologue to the final CID measurement. The use of a validated MS methodology to investigate ^{13}C-labeling dynamics within plant TCA cycle may help to strengthen our knowledge about its functioning.

A robust methodology to evaluate CID measurements and identify analytical and matrix biases

In this study, we proposed a workflow to assess the measurement accuracy of CID from TMS-derivatives of organic and amino acids by GC-MS for applications in plants, based on tailor-made *E. coli* ^{13}C biological standards with controlled patterns of CID (^{13}C-PT) (**Figure 1**). From the TMS-derivatives (selected to maximize information on carbon backbones), we showed that most of them had a remarkable accuracy, leading to very small biases in the measurement of CIDs (below 5%) and mean ^{13}C enrichments (below 1%). We further validated their suitability for application in plants by monitoring very low residual molecular ^{13}C-enrichments in Arabidopsis seedlings and *B. napus* leaves, although these accuracies could be variable between the two plant matrices (Citrate_4TMS_C1C6, Malate_3TMS_C1C4, α-Alanine_2TMS_C2C3, Aspartate_2TMS_C2C4 and Serine_3TMS). However, among amino acid TMS-derivatives, we identified three important biases at the isotopologue level. The first bias concerned the contamination of the isotopic cluster of Proline_2TMS_C2C5 at the m/z 146 (**Figure 3D**). A previous study reported this contaminant using chemical standards at natural ^{13}C abundance, but no explanation was provided for this bias (Antoniewicz et al., 2006). Here, we showed that the m/z 146 came from the co-elution with Isoleucine, *i.e.* a separation by 0.02 seconds in our chromatograms, equivalent to 0.33 °C with the ramp time for temperature during the elution (+10°C.min^{-1}). Nevertheless, this contamination only led to a slight overestimation of the M4 isotopologue (^{13}C-PT samples) (**Figure 2A**), which did not strongly impact the accuracy measurement for mean ^{13}C enrichment (**Figure 3B**). Thus, this fragment may still be suitable for ^{13}C-MFA in plants, as long as the ^{13}C-labeling strategy for the metabolic network is adapted to prevent the production of M4 isotopologues. The second bias identified concerned the contamination of the isotopic cluster of Valine_2TMS_C2C5 at the m/z 147, which was observed in both chemical standards and plant matrices. Interestingly, when a siliconium ion (loss of a methyl in a TMS group) operates a cyclization by attacking another TMS group of the same molecule, it produces an ion $[(CH^3)^3Si\text{-}O\text{-}Si(CH^3)^2]^+$ of the same mass 147 (Harvey and Vouros, 2020). We also detected a significant abundance of an m/z 246 in the fragmentation spectra of Valine_2TMS, which seems to support this hypothesis for the contamination (**Figure S2**). The third bias concerned the very high level of M1 isotopologue for Threonine_3TMS_C2C4 detected in both chemical standards and plant matrices. In its fragmentation spectra, we found an additional M1 isotopologue contamination for the peak m/z 291, an important fragment for the identification of Threonine_3TMS by GC-MS (**Figure S2**, NIST database). Given that we are working at a nominal mass resolution, we cannot determine whether this contamination is due to: i) a co-elution of a contaminant chemically similar to Threonine; ii) a strong isotopic effect during the derivatization. The use of GC coupled to high-resolution MS may help to resolve this analytical issue (instrument not available at present in our platform). Besides this, we observed a high level of M0 contamination for CID measurement of Succinate using the ^{13}C-PT full metabolites extract, that has been reported previously (Millard et al., 2014), but prevented its accurate evaluation with our workflow. Nevertheless, there was a small biological and analytical variability for Succinate_2TMS_C1C4 in our ^{13}C-labeling experiments and we measured similar ratios for M1 and M3 with Glutamate_2TMS_C2C5 that was already validated by our method (**Figure 6B**). Since M1 and M3 were both impacted by the M0 contamination in ^{13}C-PT samples, our results suggest that this fragment can be reliably used for ^{13}C-MFA in plants.

Using our validated method, we provided important information about the activity of the TCA cycle that contrasted with some proposed flux modes for TCA cycle in illuminated leaves or during a light/dark cycle (Tcherkez et al., 2009;Gauthier et al., 2010;Sweetlove et al., 2010;Tcherkez et al., 2017;da Fonseca-Pereira et al., 2021).

Stored Citrate is unlikely to contribute to TCA cycle activity in *Brassica napus* leaves

The hypothesis about the role of night-stored citrate molecules relies on few works to date. In the first work, after 50 min of $^{13}CO_2$ incorporation in *Xanthium stumarium* leaves, ^{13}C redistribution towards metabolites were used to propose "transmission coefficients" that required the contribution of an important pool of unlabeled Citrate to work (Tcherkez et al., 2009). The second work used the following experimental set-up ($^{13}CO_2$ 6h light/$^{12}CO_2$ 6h dark/$^{12}CO_2$ 6h light, with $^{15}NH_4{}^{15}NO_3$ available all the time) with *B. napus* leaves and a petiole-feeding assay (Gauthier et al., 2010). Analysis of the results by NMR showed a weak ^{13}C-enrichment for Citrate, Glutamate, Glutamine and Malate at the end of the first light period and 30 min after the beginning of the dark period compared to the end of the experiment. Combined to a higher occurrence of ^{12}C-^{15}N interactions compared to ^{13}C-^{15}N interactions in Glutamate after 6h of light with $^{13}CO_2$, the results were interpreted as evidences for the contribution of night-stored vacuolar Citrate and Malate molecules to TCA cycle activity in the subsequent light period. However, the citrate pool size was not monitored and the ^{13}C enrichment of TCA cycle metabolites at the end of the dark period and/or at the beginning of the second light period remained unknown. Nevertheless, these results were then partly supported by a flux balance analysis using a diel model which explained this stored citrate contribution by the need to support continued export of sugar and amino acids from the leaf during the night and to meet cellular maintenance costs (Cheung et al., 2014). Recently, this concept has been reinforced by the subcellular distribution of Citrate in plant leaves, which is essentially present in the vacuoles (Destailleur et al., 2021). However, previous NMR works used detached leaves to propose the contribution of the stored citrate, which is an experimental setup that necessarily stops sink/source relationships (sugar and amino acids exports) (Gauthier et al., 2010). Thus, the light/dark regulation of the stored citrate contribution should be observed in both detached leaves and leaf discs. Here, using *B. napus* leaf discs and a U-^{13}C-pyruvate labeling incorporation, we provided evidences for the absence of stored Citrate contribution to the TCA cycle in a light/dark dependent manner (**Figure 8**). First, we showed that the M2/(M0+M2) ratio of the Acetyl-CoA active pool was close to 0.4 after 4 to 6 hours in our experiments, thereby showing that most of M0 isotopologues from active pools of TCA cycle metabolites came from M0 Acetyl-CoA and M0 OAA and not a stored pool of ^{12}C-Citrate (**Figure 6B**). Given the important production of PEPc-derived molecules with non-labeled PEP in our experiments, ^{12}C-Pyruvate may have been produced by the glycolysis during our kinetic, thereby diluting the mitochondrial U-^{13}C-Pyruvate pool (nearly 20% of M0 still detected for the Pyruvate poll at the leaf level). However, it is also possible that the thioredoxin-mediated activation of the ATP citrate lyase activity in light conditions leads to the conversion of stored ^{12}C-Citrate pool into ^{12}C-OAA and ^{12}C-Acetyl-CoA (Sweetlove et al., 2010;da Fonseca-Pereira et al., 2021). In our experiments, the ^{13}C-enrichment of Acetyl-CoA was calculated from ^{13}C-labeled fragments of either Succinate or Glutamate (independent of their ^{12}C-molecules (M0 isotopologues)), thus this measurement can only be biased if there is a contribution of stored ^{12}C-Citrate converted to ^{12}C-Acetyl-CoA. However, if such contribution was relatively important in the light and negligible in the dark (concept of the stored citrate contribution), it would necessarily introduce a ^{12}C isotopic dilution for mean ^{13}C enrichment of Glutamate and Succinate in the light compared to the dark (Gauthier et al., 2010), and this was not observed here while the system was in a metabolic steady-state (**Figure 4**). Second, we did not observe any significant modification of the Citrate pool during the 6 hours of our experiment (**Figure 4B, Table S4**) while a strong decrease in light conditions and a strong increase in dark conditions were expected with the hypothesis of the stored citrate remobilization

(Cheung et al., 2014). Altogether, our results showed that the contribution of stored citrate to the TCA cycle activity is unlikely to occur in *B. napus* leaves (**Figure 8**).

The forward cyclic flux mode of the TCA cycle has a higher contribution to Malate biosynthesis compared to PEPc in *Brassica napus* leaves

The non-cyclic nature of the TCA cycle has been previously proposed in illuminated leaves from works that used different experimental setup/labeling strategies. This non-cyclic nature in the light was mostly explained by the need to sustain *de novo* nitrogen assimilation and was supported by higher PEPc activities compared to dark conditions (Gauthier et al., 2010;Caburatan and Park, 2021). A first experiment was based on detached leaves of *Xanthium stumarium* and ^{13}C labeling with either $^{13}C_1$-pyruvate or U-^{13}C-Pyruvate (Tcherkez et al., 2009). The authors did not observe a significant ^{13}C enrichment in the Succinate compared to Fumarate with a 2-hour $^{13}C_1$-pyruvate incorporation while both metabolites showed similar ^{13}C-enrichments with a 2-hour U-^{13}C-Pyruvate incorporation. However, the reassimilation of $^{13}CO_2$ from $^{13}C_1$-Pyruvate decarboxylation by PEPc cannot be metabolically transmitted from Malate to Succinate since the C1 and the C4 of the OAA backbone are lost during Citrate to Succinate conversion (**Figure 6A**) (Alves et al., 2015;Lima et al., 2021). Three other experiments were based on 1-hour $^{13}CO_2$ labeling with either detached or attached leaves from *Xanthium stumarium*, Arabidopsis or *Camelina sativa* (Tcherkez et al., 2009;Xu et al., 2021;Xu et al., 2022). The two INST-MFA approaches notably predicted that PEPc and the pyruvate-to-2-oxoglutarate conversion experienced both relatively similar metabolic fluxes (ratio close to 1), while the flux from 2-oxoglutarate to succinate and from OAA to malate were both equal to 0. Thus, these previous works never identified the relative contribution of PEPc and TCA cycle to Malate biosynthesis. Perhaps, this can be partly attributed to the ^{13}C labeling strategy: $^{13}CO_2$ must be quickly assimilated by the PEPc thanks to the anhydrase carbonic while the $^{13}CO_2$ fixed by the RuBiSCO will require more time to be transmitted to PEP and pyruvate (See the dynamics of CIDs for Trioses phosphates, Alanine, Citrate and Aspartate therein (Xu et al., 2021)). Consequently, ^{13}C enrichment could be artificially higher in Citrate and Glutamate compared to Succinate with this $^{13}CO_2$ labeling strategy (C1 and the C4 of the OAA backbone are lost during Citrate to Succinate conversion (**Figure 6A**)).

Here, we assessed the flux modes of the TCA Cycle by taking advantage of pathway-specific mass isotopologues/isotopomers and a ^{13}C-MFA approach after a U-^{13}C-Pyruvate incorporation in *B. napus* leaf discs. This approach was notably based on the simultaneous application of ^{13}C labeling thanks to the PDH that produced $^{13}C_2$-AcetylCoA for the TCA cycle and $^{13}CO_2$ for the PEPc. Interestingly, we showed that Glutamate and Succinate rapidly harbored M2 istopologues, corresponding to *de novo* incorporation of M2 Acetyl-CoA from the TCA Cycle, followed by an increase of M1 and M3 isotopologues that were clearly visible after only 2 hours. These isotopologues corresponded to M2 isotopologues that had experienced a complete turn of the forward cyclic mode of the TCA cycle. They provided for the first time in plants a unique ^{13}C-labeling signature following U-^{13}C-pyruvate incorporation that demonstrated the cyclic nature of the plant TCA cycle in *B. napus* leaves (**Figure 5**). From these results, we combined a ^{13}C-MFA approach with pathway specific MS fragments and the indirect measurement of M2/(M0+M2) ratio for the Acetyl-CoA active pool to show that the forward cyclic mode of the TCA cycle contributed to nearly 80% of both Malate and Citrate production compared to PEPc (4:1 activity ratio) in both light and dark conditions with our experimental setup, while malic enzyme activity was not significantly detected (**Figure 6**). One may question the use of pyruvate for ^{13}C labeling strategies, since it may introduce an artificial increase of TCA cycle turn-over compared to experiments with $^{13}CO_2$. This could ultimately lead to important ^{13}C enrichments for Succinate and the rapid apparition of M1 and M3 isotopologues for Glutamate and Succinate. A recent

incorporation of 15 mM U-^{13}C-pyruvate or 15 mM U-^{13}C-glucose into Arabidopsis with a petiole feeding assay during 4 hours in the light identified important ^{13}C enrichments in Citrate, Glutamate and Succinate (Zhang et al., 2021). However, another experiment (Arabidopsis leaf discs, 20 mM U-^{13}C-pyruvate, up to 8 hours in the dark) showed similar results but only observed M2 isotopologues for Citrate, Glutamate and Succinate and not M1 and M3 isotopologues which were expected for a cyclic mode (complete dataset available on request from the authors) (Le et al., 2021). Thus, the use of pyruvate does not seem to artificially increase the turn-over of the TCA cycle in Arabidopsis, *i.e.* metabolites experiencing multiples turns of the TCA cycle. Therefore, the forward cyclic mode of the TCA cycle has definitely a higher contribution to Malate biosynthesis compared to PEPc in *B. napus* leaves. Nevertheless, this TCA cycle/PEPc ratio (4:1) may have been slightly overestimated in our study since this pathway fractional contribution assumes that most of the CO_2 is produced by the PDH, and its conversion to HCO_3^- are not rate-limiting for PEPc activity. While the second hypothesis may not be so constraining given that CO_2 was actively reassimilated by photosynthesis in our light conditions (**Figure 7**), the second hypothesis can be questioned given the metabolic network (**Figure 6**). Indeed, isocitrate and 2-oxoglutarate dehydrogenases necessarily decarboxylate more $^{12}CO_2$ than $^{13}CO_2$ compared to the PDH (see mean ^{13}C enrichment of metabolically active pool of Acetyl-CoA, **Figure 6B**). This could imbalance the reassimilation of $^{13}CO_2$ by PEPc if the first part of the TCA cycle operates at a rate close to the PEPc activity. Assuming an equivalent metabolic flux from PDH to 2-oxoglutarate dehydrogenase based on previous works with $^{13}CO_2$ (Xu et al., 2021;Xu et al., 2022), the overall mitochondrial $^{12}CO_2/^{13}CO_2$ ratio should not exceed a 2:1 dilution compared to the $^{12}CO_2/^{13}CO_2$ produced by the PDH (see CID of Citrate, Glutamate and Succinate and their associated CO_2 losses). Thus, the forward cyclic mode of the TCA cycle will still majorly contribute to Malate and Citrate production compared to PEPc in our experimental setup with this scenario (a 2:1 ratio is expected) (**Figure 8**). Interestingly, a ^{13}C-MFA performed at isotopic and metabolic steady-state in heterotrophic suspension cells culture incubated with U-^{13}C-glucose showed a similar ratio of 2:1 for forward TCA cycle/PEPc metabolic fluxes (ana1 versus tca2, tca3, tca4, tca5), with a negligible malic enzyme activity (10-fold less than PEPc) (Masakapalli et al., 2010).

Besides this, the forward cyclic mode of the TCA cycle has to be reconnected to the relative ^{13}C content found in Glutamate and Aspartate in our study. This can represent important escapes for ^{13}C, thereby driving the relative differences of metabolic flux for the biosynthesis of Glutamate and Succinate, and Malate and OAA respectively (branching points) (**Figure 5**). Nevertheless, a significant proportion of Glutamate and Aspartate may come back to the TCA cycle. In astrocyte cells, U-^{13}C-Glutamate labeling incorporations showed that Glutamate M5 was rapidly metabolized into Glutamate M3 after one turn of the TCA cycle (Nissen et al., 2015) thereby proposing a similar role for plant mitochondrial Glutamate dehydrogenase (Terce-Laforgue et al., 2013). The potential role of GABA (Gamma-aminobutyric acid) shunt has been proposed to reroute Glutamate towards Succinate (Tcherkez et al., 2009). Finally, mitochondrial transaminases such as Alanine:2-oxoglutarate and Aspartate:2-oxoglutarate could also participle in this process. Indeed, Alanine:2-oxoglutarate aminotransferase is one of the three pathway supplying pyruvate to mitochondria and was notably solicited in the *mpc1* mutants to compensate for the loss of mitochondrial pyruvate import (Le et al., 2021). Regarding Glutamate, its production from ^{13}C-2-Oxoglutarate and ^{12}C-Glutamine molecules in our metabolic network will necessarily introduce a 50% isotopic dilution between ^{12}C and ^{13}C molecules. Thus, its reassimilation will also introduce this 50% isotopic dilution to mitochondrial active pools of either Succinate or 2-Oxoglutarate. For instance, it is not possible to have access to the size of the mitochondrial active pool for both metabolites and by extension their exact ^{13}C-enrichments without a complete isotopic steady-state of the plant TCA cycle and perhaps subcellular fractionation or very fast mitochondrial purification by centrifugation (Lee et al., 2019;Destailleur et al., 2021). To which extent Glutamate and Aspartate molecules escape the TCA cycle remains to be determined.

Light/dark regulation of PEPc and TCA cycle contributions to Malate and Citrate biosynthesis in *Brassica napus* leaves

PEPc activity is positively regulated by its light-dependent thioredoxin-mediated phosphorylation in C_3 and C_4 plants (Caburatan and Park, 2021). Thus, PEPc is expected to be more active in the light than in the dark, as recently suggested in guard cell cultures based on the differential ^{13}C enrichment found for the C1 of Glutamate (Lima et al., 2021). Here, we focused our analysis on both Malate and Citrate to compare PEPc and TCA cycle contribution to their biosynthesis. We notably showed that Malate_3TMS_C1C4 fragment experienced a strong shift in its M1/M2 isotopologues in light conditions compared to dark conditions (**Figure 5**). This was associated to a relatively higher contribution of PEPc to Malate production in light conditions compared to dark conditions (**Figure 6B**). However, such shift could be attributed to both increased PEPc activity and TCA cycle inhibition in the light. In our experiments, we found very similar dynamics of ^{13}C-enrichment for TCA cycle metabolites in both dark and light conditions combined to similar metabolic pool sizes in a metabolic steady-state (**Figure 4**). Thus, variations of TCA cycle metabolic fluxes between light and dark conditions are expected to be very low in our experimental set-up. Since we used 10 mM U-^{13}C-pyruvate for labeling experiments, perhaps this has activated the PDH thereby eliminating one of the major bottlenecks regulating the entry of carbon for plant TCA cycle. A previous work based on $^{13}CO_2$ decarboxylations with either ^{13}C-pyruvate or ^{13}C-glucose showed that PDH was inhibited by up to 27% in the light compared to the dark, while glycolysis could be inhibited by up to 95% (Tcherkez et al., 2005). However, these inhibitions were necessarily underestimated by the measurement method which did not considered the reassimilation of $^{13}CO_2$ by the RuBiSCO. Here, by integrating a ^{13}C-positionnal isotopomer approach to the photorespiratory metabolism, we showed that PDH and TCA-cycle derived CO_2 were actively reassimilated by the RuBiSCO, leading to a contribution of around 5% to net CO_2 assimilation (**Figure 7**). Under the light irradiance of around 120 µmol photons.$m^{-2}.s^{-1}$ (same light intensity of our experimental setup), net CO_2 uptake of *B. napus* leaves at a similar developmental stage (L11 and L7 leaves) is close to 5 µmol CO_2. $m^{-2}.s^{-1}$ (Dellero et al., 2021), leading to a reassimilation rate of 0.25 µmol CO_2. $m^{-2}.s^{-1}$. Since the dark respiration rate for these leaves is close to 1.25 µmol CO_2. $m^{-2}.s^{-1}$ (Dellero et al., 2021), and given the proposed inhibition of mitochondrial respiration by nearly 50% in the light (Tcherkez et al., 2005), this will give a day respiration rate of 0.625 µmol CO_2. $m^{-2}.s^{-1}$, but without considering the reassimilation rate of PDH and TCA-derived decarboxylations. Therefore, the current measurement/estimation of day respiration rate through CO_2 mass balance at the leaf level (Tcherkez et al., 2017;Berghuijs et al., 2019) must be underestimated by nearly 40% (0.875 versus 0.625). Thus, the inhibition of day respiration at the metabolic flux level is likely be lower than measured by gas-exchanges and could only represent 30% in our experiments (1.25 in the dark versus 0.875 in the light) (**Figure 8**). Besides this, the *pdk* mutant responsible for the activation of the PDH in the light was recently used for ^{13}C labeling experiments. After a U-^{13}C-pyruvate incorporation into Arabidopsis leaves during 4 hours in the light, the *pdk* mutant had higher ^{13}C-enrichments for Citrate, Glutamate and Succinate compared to the control (Zhang et al., 2021). However, there were no differences when using U-^{13}C-Glucose. This result questioned the regulatory power of the PDH for the activity of the TCA cycle in the light, especially when carbon arising from glycolysis is not limiting. Based on these observations, we think that the similar dynamics of ^{13}C-enrichment observed in our experiments for light and dark conditions are essentially explained by the elimination of the light/dark regulation of glycolysis. Since the inhibition of PDH and TCA cycle decarboxylations in the light (50%) is supposed to be close to 30% only at the metabolic flux level, the fractional contributions calculated before have necessarily overestimated the contribution of the TCA cycle in light conditions by up to 30% compared to dark conditions. Nevertheless, the forward cyclic flux mode of the TCA cycle will still have a major contribution to Malate and Citrate biosynthesis compared to PEPc (ratio 4:1 would be close to 3:1 after correction). Therefore, the shift in M1/M2

isotopologues of Malate_3TMS_C1C4 fragment in light conditions compared to dark conditions essentially captured the light/dark regulation of PEPc.

Besides this, we observed another unexpected but interesting result: the higher contribution of PEPc derived-carbons to Citrate production in the dark condition compared to the light condition. Since we have shown that PEPc contribution to Malate production was reduced in the dark compared to the light, this result can only be explained by a higher transport of OAA/Malate from the cytosol to the mitochondria in dark conditions (**Figure 8**). This idea is supported by the fact that PEPc is majorly localized to the cytosol (Caburatan and Park, 2021) and the recent identification of a mitochondrial malate importer in Arabidopsis with an important impact on mitochondrial respiration in the dark (Lee et al., 2021). Whether a higher malate import into mitochondria allows to increase the absolute metabolic flux of the TCA cycle in dark conditions in our experimental set-up remains to be elucidated.

Conclusions

Overall, we proposed a robust workflow to evaluate the accuracy of CID measurements by GC-MS for organic and amino acids and successfully applied our validated method to the investigation of TCA cycle and PEPc metabolic fluxes in *Brassica napus* leaves. Notably, our results did not support the hypothesis of the stored citrate contribution to TCA cycle in a light/dark-dependent manner and demonstrated that the forward cyclic flux mode of the TCA cycle largely contributed to Malate and Citrate production compared to PEPc (4:1 ratio) in *B. napus* leaves. Thus, the activity of the succinate dehydrogenase in both dark and light conditions has been largely underestimated until now. Reassimilation of PDH and TCA-cycle derived CO_2 by photosynthesis represented nearly 5% of the net CO_2 assimilation rate in our conditions, and this should be considered when day respiration rate is measured by CO_2 mass balance at the leaf level (underestimation by nearly 40%). Although the regulation of the PEPc activity by light was still operating, the higher involvement of PEPc-derived carbons to citrate production in dark conditions proposed an important role for Malate import into mitochondria in sustaining TCA cycle in dark conditions. The next stage of this work will be focused on the accurate modeling of this metabolic network to infer absolute metabolic fluxes. This perspective sounds stimulating given the development of multiple modeling approaches over the last decade but still remains highly challenging (Kruger and Ratcliffe, 2021).

5 Conflict of Interest

The authors declare that the research was conducted in the absence of any commercial or financial relationships that could be construed as a potential conflict of interest.

6 Author Contributions

Conceptualization, Y.D., A.B.; methodology, Y.D..; software, Y.D., O.F.; validation, Y.D., S.B. and C.B.; formal analysis, Y.D.; investigation, Y.D., S.B. and C.B.; data curation, Y.D.; writing-original draft preparation, Y.D.; writing-review and editing, Y.D., A.B.; visualization, Y.D.; supervision, Y.D.; project administration, Y.D.; funding acquisition, Y.D., A.B. All authors have read and agreed to the published version of the manuscript.

7 Funding

This research was supported by the IB2021_TRICYCLE project funded by the INRAE BAP division and by the METABOHUB project funded by the program Investments for the Future of the French national agency for research (ANR grant number 11-INBS-0010).

8 Acknowledgments

P2M2 (Metabolic Profiling & Metabolomics Platform, Le Rheu, France, www6.inrae.fr/p2m2/) and its staff members are gratefully acknowledged for access to mass spectrometry facilities and for supporting the methodological developments required for this study. We thank MetaToul (Metabolomics & Fluxomics Facitilies, Toulouse, France, www.metatoul.fr) for technical support and access to NMR facilities. We are grateful to Nathalie Marnet and Mathieu Aubert for technical assistance in the quantification of amino acid content and Pierre Millard and Floriant Bellvert for fruitful scientific discussions.

9 Supplementary Material

Supplementary Material available with the files deposited.

10 References

Abadie, C., Bathellier, C., and Tcherkez, G. (2018). Carbon allocation to major metabolites in illuminated leaves is not just proportional to photosynthesis when gaseous conditions (CO2 and O2) vary. *New Phytol* 218**,** 94-106.

Abadie, C., Boex-Fontvieille, E.R., Carroll, A.J., and Tcherkez, G. (2016). In vivo stoichiometry of photorespiratory metabolism. *Nat Plants* 2**,** 15220.

Abadie, C., Lothier, J., Boex-Fontvieille, E., Carroll, A., and Tcherkez, G. (2017). Direct assessment of the metabolic origin of carbon atoms in glutamate from illuminated leaves using (13) C-NMR. *New Phytol* 216**,** 1079-1089.

Abadie, C., and Tcherkez, G. (2019a). In vivo phosphoenolpyruvate carboxylase activity is controlled by CO2 and O2 mole fractions and represents a major flux at high photorespiration rates. *New Phytol* 221**,** 1843-1852.

Abadie, C., and Tcherkez, G. (2019b). Plant sulphur metabolism is stimulated by photorespiration. *Commun Biol* 2**,** 379.

Abadie, C., and Tcherkez, G. (2021). (13)C Isotope Labelling to Follow the Flux of Photorespiratory Intermediates. *Plants (Basel)* 10.

Allen, D.K., and Young, J.D. (2019). Tracing metabolic flux through time and space with isotope labeling experiments. *Curr Opin Biotechnol* 64**,** 92-100.

Alves, T.C., Pongratz, R.L., Zhao, X., Yarborough, O., Sereda, S., Shirihai, O., Cline, G.W., Mason, G., and Kibbey, R.G. (2015). Integrated, Step-Wise, Mass-Isotopomeric Flux Analysis of the TCA Cycle. *Cell Metab* 22**,** 936-947.

Antoniewicz, M.R. (2021). A guide to metabolic flux analysis in metabolic engineering: Methods, tools and applications. *Metab Eng* 63**,** 2-12.

Antoniewicz, M.R., Kelleher, J.K., and Stephanopoulos, G. (2006). Determination of confidence intervals of metabolic fluxes estimated from stable isotope measurements. *Metab Eng* 8**,** 324-337.

Antoniewicz, M.R., Kelleher, J.K., and Stephanopoulos, G. (2007). Accurate Assessment of Amino Acid Mass Isotopomer Distributions for Metabolic Flux Analysis. *Anal Chem* 79**,** 6.

Araujo, W.L., Nunes-Nesi, A., Nikoloski, Z., Sweetlove, L.J., and Fernie, A.R. (2012). Metabolic control and regulation of the tricarboxylic acid cycle in photosynthetic and heterotrophic plant tissues. *Plant Cell Environ* 35**,** 1-21.

Araujo, W.L., Tohge, T., Nunes Nesi, A., Obata, T., and Fernie, A. (2014). "Analysis of Kinetic Labeling of Amino Acids and Organic Acids by GC-MS," in *Plant Metabolic Flux Analysis: Methods and Protocols*, ed. M.I.M. Biology.).

Berghuijs, H.N.C., Yin, X., Ho, Q.T., Retta, M.A., Nicolai, B.M., and Struik, P.C. (2019). Using a reaction-diffusion model to estimate day respiration and reassimilation of (photo)respired CO2 in leaves. *New Phytol* 223**,** 619-631.

Bianchetti, G., Baron, C., Carrillo, A., Berardocco, S., Marnet, N., Wagner, M.H., Demilly, D., Ducournau, S., Manzanares-Dauleux, M.J., Caherec, F.L., Buitink, J., and Nesi, N. (2021). Dataset for the metabolic and physiological characterization of seeds from oilseed rape (Brassica napus L.) plants grown under single or combined effects of drought and clubroot pathogen Plasmodiophora brassicae. *Data Brief* 37**,** 107247.

Buescher, J.M., Antoniewicz, M.R., Boros, L.G., Burgess, S.C., Brunengraber, H., Clish, C.B., Deberardinis, R.J., Feron, O., Frezza, C., Ghesquiere, B., Gottlieb, E., Hiller, K., Jones, R.G., Kamphorst, J.J., Kibbey, R.G., Kimmelman, A.C., Locasale, J.W., Lunt, S.Y., Maddocks, O.D., Malloy, C., Metallo, C.M., Meuillet, E.J., Munger, J., Noh, K., Rabinowitz, J.D., Ralser, M., Sauer, U., Stephanopoulos, G., St-Pierre, J., Tennant, D.A., Wittmann, C., Vander Heiden, M.G., Vazquez, A., Vousden, K., Young, J.D., Zamboni, N., and Fendt, S.M. (2015). A roadmap for interpreting (13)C metabolite labeling patterns from cells. *Curr Opin Biotechnol* 34**,** 189-201.

Caburatan, L., and Park, J. (2021). Differential Expression, Tissue-Specific Distribution, and Posttranslational Controls of Phosphoenolpyruvate Carboxylase. *Plants (Basel)* 10.

Cheah, Y.E., Xu, Y., Sacco, S.A., Babele, P.K., Zheng, A.O., Johnson, C.H., and Young, J.D. (2020). Systematic identification and elimination of flux bottlenecks in the aldehyde production pathway of Synechococcus elongatus PCC 7942. *Metab Eng* 60**,** 56-65.

Cheah, Y.E., and Young, J.D. (2018). Isotopically nonstationary metabolic flux analysis (INST-MFA): putting theory into practice. *Curr Opin Biotechnol* 54**,** 80-87.

Cheung, C.Y., Poolman, M.G., Fell, D.A., Ratcliffe, R.G., and Sweetlove, L.J. (2014). A Diel Flux Balance Model Captures Interactions between Light and Dark Metabolism during Day-Night Cycles in C3 and Crassulacean Acid Metabolism Leaves. *Plant Physiol* 165**,** 917-929.

Clark, T.J., Guo, L., Morgan, J., and Schwender, J. (2020). Modeling Plant Metabolism: From Network Reconstruction to Mechanistic Models. *Annu Rev Plant Biol*.

Da Fonseca-Pereira, P., Souza, P.V.L., Fernie, A.R., Timm, S., Daloso, D.M., and Araujo, W.L. (2021). Thioredoxin-mediated regulation of (photo)respiration and central metabolism. *J Exp Bot* 72**,** 5987-6002.

Daloso, D.M., Medeiros, D.B., Dos Anjos, L., Yoshida, T., Araujo, W.L., and Fernie, A.R. (2017). Metabolism within the specialized guard cells of plants. *New Phytol* 216**,** 1018-1033.

Dellero, Y. (2020). Manipulating amino acid metabolism to improve crop nitrogen use efficiency for a sustainable agriculture. *Frontiers in Plant Science* 11**,** 1857

Dellero, Y., Clouet, V., Marnet, N., Pellizzaro, A., Dechaumet, S., Niogret, M.F., and Bouchereau, A. (2020a). Leaf status and environmental signals jointly regulate proline metabolism in winter oilseed rape. *J Exp Bot* 71**,** 2098-2111.

Dellero, Y., and Filangi, O. (2021). "Corrective method dedicated to Isocor for calculating carbon isotopologue distribution from GCMS runs". V1 ed.: Portail Data INRAE).

Dellero, Y., Heuillet, M., Marnet, N., Bellvert, F., Millard, P., and Bouchereau, A. (2020b). Sink/Source Balance of Leaves Influences Amino Acid Pools and Their Associated Metabolic Fluxes in Winter Oilseed Rape (Brassica napus L.). *Metabolites* 10**,** 16.

Dellero, Y., Jossier, M., Bouchereau, A., Hodges, M., and Leport, L. (2021). Leaf Phenological Stages of Winter Oilseed Rape (Brassica napus L.) Have Conserved Photosynthetic Efficiencies but Contrasted Intrinsic Water Use Efficiencies at High Light Intensities. *Frontiers in Plant Science* 12.

Dellero, Y., Jossier, M., Glab, N., Oury, C., Tcherkez, G., and Hodges, M. (2016). Decreased glycolate oxidase activity leads to altered carbon allocation and leaf senescence after a transfer from high CO2 to ambient air in Arabidopsis thaliana. *J Exp Bot* 67**,** 3149-3163.

Destailleur, A., Poucet, T., Cabasson, C., Alonso, A.P., Cocuron, J.C., Larbat, R., Vercambre, G., Colombie, S., Petriacq, P., Andrieu, M.H., Beauvoit, B., Gibon, Y., and Dieuaide-Noubhani, M. (2021). The Evolution of Leaf Function during Development Is Reflected in Profound Changes in the Metabolic Composition of the Vacuole. *Metabolites* 11.

Dong, H., Bai, L., Zhang, Y., Zhang, G., Mao, Y., Min, L., Xiang, F., Qian, D., Zhu, X., and Song, C.P. (2018). Modulation of Guard Cell Turgor and Drought Tolerance by a Peroxisomal Acetate-Malate Shunt. *Mol Plant* 11**,** 1278-1291.

Evers, B., Gerding, A., Boer, T., Heiner-Fokkema, M.R., Jalving, M., Wahl, S.A., Reijngoud, D.J., and Bakker, B.M. (2021). Simultaneous Quantification of the Concentration and Carbon Isotopologue Distribution of Polar Metabolites in a Single Analysis by Gas Chromatography and Mass Spectrometry. *Anal Chem* 93**,** 8248-8256.

Galili, G., Amir, R., and Fernie, A.R. (2016). The Regulation of Essential Amino Acid Synthesis and Accumulation in Plants. *Annu Rev Plant Biol* 67**,** 153-178.

Gauthier, P.P., Bligny, R., Gout, E., Mahe, A., Nogues, S., Hodges, M., and Tcherkez, G.G. (2010). In folio isotopic tracing demonstrates that nitrogen assimilation into glutamate is mostly independent from current CO2 assimilation in illuminated leaves of Brassica napus. *New Phytol* 185**,** 988-999.

Harvey, D.J., and Vouros, P. (2020). Mass Spectrometric Fragmentation of Trimethylsilyl and Related Alkylsilyl Derivatives. *Mass Spectrom Rev* 39**,** 105-211.

Hay, J.O., Shi, H., Heinzel, N., Hebbelmann, I., Rolletschek, H., and Schwender, J. (2014). Integration of a constraint-based metabolic model of Brassica napus developing seeds with (13)C-metabolic flux analysis. *Front Plant Sci* 5**,** 724.

Heise, R., Fernie, A.R., Stitt, M., and Nikoloski, Z. (2015). Pool size measurements facilitate the determination of fluxes at branching points in non-stationary metabolic flux analysis: the case of Arabidopsis thaliana. *Front Plant Sci* 6**,** 386.

Heuillet, M., Bellvert, F., Cahoreau, E., Letisse, F., Millard, P., and Portais, J.C. (2018). Methodology for the Validation of Isotopic Analyses by Mass Spectrometry in Stable-Isotope Labeling Experiments. *Anal Chem* 90**,** 1852-1860.

Heuillet, M., Millard, P., Cisse, M.Y., Linares, L.K., Letisse, F., Manie, S., Le Cam, L., Portais, J.C., and Bellvert, F. (2020). Simultaneous Measurement of Metabolite Concentration and Isotope Incorporation by Mass Spectrometry. *Anal Chem*.

Kambhampati, S., Li, J., Evans, B.S., and Allen, D.K. (2019). Accurate and efficient amino acid analysis for protein quantification using hydrophilic interaction chromatography coupled tandem mass spectrometry. *Plant Methods* 15**,** 46.

Kruger, N.J., Huddleston, J.E., Le Lay, P., Brown, N.D., and Ratcliffe, R.G. (2007). Network flux analysis: impact of 13C-substrates on metabolism in Arabidopsis thaliana cell suspension cultures. *Phytochemistry* 68**,** 2176-2188.

Kruger, N.J., and Ratcliffe, R.G. (2015). Fluxes through plant metabolic networks: measurements, predictions, insights and challenges. *Biochem J* 465**,** 27-38.

Kruger, N.J., and Ratcliffe, R.G. (2021). Whither metabolic flux analysis in plants? *Journal of Experimental Botany*.

Lai, Z., and Fiehn, O. (2018). Mass spectral fragmentation of trimethylsilylated small molecules. *Mass Spectrom Rev* 37**,** 245-257.

Le, X.H., Lee, C.P., and Millar, A.H. (2021). The mitochondrial pyruvate carrier (MPC) complex mediates one of three pyruvate-supplying pathways that sustain Arabidopsis respiratory metabolism. *Plant Cell* 33**,** 2776-2793.

Lee, C.P., Elsasser, M., Fuchs, P., Fenske, R., Schwarzlander, M., and Millar, A.H. (2021). The versatility of plant organic acid metabolism in leaves is underpinned by mitochondrial malate-citrate exchange. *Plant Cell* 33**,** 3700-3720.

Lee, W.D., Mukha, D., Aizenshtein, E., and Shlomi, T. (2019). Spatial-fluxomics provides a subcellular-compartmentalized view of reductive glutamine metabolism in cancer cells. *Nat Commun* 10**,** 1351.

Lima, V.F., Erban, A., Daubermann, A.G., Freire, F.B.S., Porto, N.P., Candido-Sobrinho, S.A., Medeiros, D.B., Schwarzlander, M., Fernie, A.R., Dos Anjos, L., Kopka, J., and Daloso, D.M. (2021). Establishment of a GC-MS-based (13) C-positional isotopomer approach suitable for investigating metabolic fluxes in plant primary metabolism. *Plant J*.

Lima, V.F., Perez Souza, L., Williams, T.C., Fernie, A., and Daloso, D.M. (2018). "Gas Chromatography–Mass Spectrometry-Based 13C-Labeling Studies in Plant Metabolomics," in *Plant Metabolomics: Methods and Protocol*, ed. M.I.M. Biology.).

Ma, F., Jazmin, L.J., Young, J.D., and Allen, D.K. (2014). Isotopically nonstationary 13C flux analysis of changes in Arabidopsis thaliana leaf metabolism due to high light acclimation. *Proc Natl Acad Sci U S A* 111**,** 16967-16972.

Masakapalli, S.K., Le Lay, P., Huddleston, J.E., Pollock, N.L., Kruger, N.J., and Ratcliffe, R.G. (2010). Subcellular flux analysis of central metabolism in a heterotrophic Arabidopsis cell suspension using steady-state stable isotope labeling. *Plant Physiol* 152**,** 602-619.

Medeiros, D.B., Perez Souza, L., Antunes, W.C., Araujo, W.L., Daloso, D.M., and Fernie, A.R. (2018). Sucrose breakdown within guard cells provides substrates for glycolysis and glutamine biosynthesis during light-induced stomatal opening. *Plant J* 94**,** 583-594.

Millard, P., Cahoreau, E., Heuillet, M., Portais, J.C., and Lippens, G. (2017). (15)N-NMR-Based Approach for Amino Acids-Based (13)C-Metabolic Flux Analysis of Metabolism. *Anal Chem* 89**,** 2101-2106.

Millard, P., Delepine, B., Guionnet, M., Heuillet, M., Bellvert, F., and Letisse, F. (2019). IsoCor: isotope correction for high-resolution MS labeling experiments. *Bioinformatics* 35**,** 4484-4487.

Millard, P., Massou, S., Portais, J.C., and Letisse, F. (2014). Isotopic studies of metabolic systems by mass spectrometry: using Pascal's triangle to produce biological standards with fully controlled labeling patterns. *Anal Chem* 86**,** 10288-10295.

Millard, P., Schmitt, U., Kiefer, P., Vorholt, J.A., Heux, S., and Portais, J.-C. (2020). ScalaFlux: a scalable approach to quantify fluxes in metabolic subnetworks. *Plos Computational Biology* 16**,** e1007799.

Nissen, J.D., Pajecka, K., Stridh, M.H., Skytt, D.M., and Waagepetersen, H.S. (2015). Dysfunctional TCA-Cycle Metabolism in Glutamate Dehydrogenase Deficient Astrocytes. *Glia* 63**,** 2313-2326.

Okahashi, N., Kawana, S., Iida, J., Shimizu, H., and Matsuda, F. (2019). Fragmentation of Dicarboxylic and Tricarboxylic Acids in the Krebs Cycle Using GC-EI-MS and GC-EI-MS/MS. *Mass Spectrom (Tokyo)* 8**,** A0073.

Ratcliffe, R.G., and Shachar-Hill, Y. (2006). Measuring multiple fluxes through plant metabolic networks. *Plant J* 45**,** 490-511.

Rstudio Team (2016). RStudio: Integrated Development for R.

.

Sinnaeve, D., Dinclaux, M., Cahoreau, E., Millard, P., Portais, J.C., Letisse, F., and Lippens, G. (2018). Improved Isotopic Profiling by Pure Shift Heteronuclear 2D J-Resolved NMR Spectroscopy. *Anal Chem* 90**,** 4025-4031.

Sweetlove, L.J., Beard, K.F., Nunes-Nesi, A., Fernie, A.R., and Ratcliffe, R.G. (2010). Not just a circle: flux modes in the plant TCA cycle. *Trends Plant Sci* 15**,** 462-470.

Szecowka, M., Heise, R., Tohge, T., Nunes-Nesi, A., Vosloh, D., Huege, J., Feil, R., Lunn, J., Nikoloski, Z., Stitt, M., Fernie, A.R., and Arrivault, S. (2013). Metabolic fluxes in an illuminated Arabidopsis rosette. *Plant Cell* 25**,** 694-714.

Tcherkez, G., Cornic, G., Bligny, R., Gout, E., and Ghashghaie, J. (2005). In vivo respiratory metabolism of illuminated leaves. *Plant Physiol* 138**,** 1596-1606.

Tcherkez, G., Gauthier, P., Buckley, T.N., Busch, F.A., Barbour, M.M., Bruhn, D., Heskel, M.A., Gong, X.Y., Crous, K.Y., Griffin, K., Way, D., Turnbull, M., Adams, M.A., Atkin, O.K., Farquhar, G.D., and Cornic, G. (2017). Leaf day respiration: low CO2 flux but high significance for metabolism and carbon balance. *New Phytol* 216**,** 986-1001.

Tcherkez, G., Mahe, A., Gauthier, P., Mauve, C., Gout, E., Bligny, R., Cornic, G., and Hodges, M. (2009). In folio respiratory fluxomics revealed by 13C isotopic labeling and H/D isotope effects highlight the noncyclic nature of the tricarboxylic acid "cycle" in illuminated leaves. *Plant Physiol* 151**,** 620-630.

Terce-Laforgue, T., Bedu, M., Dargel-Grafin, C., Dubois, F., Gibon, Y., Restivo, F.M., and Hirel, B. (2013). Resolving the role of plant glutamate dehydrogenase: II. Physiological characterization of plants overexpressing the two enzyme subunits individually or simultaneously. *Plant Cell Physiol* 54**,** 1635-1647.

Timm, S. (2020). The impact of photorespiration on plant primary metabolism through metabolic and redox regulation. *Biochemical Society Transactions* 48**,** 2495-2504.

Treves, H., Kuken, A., Arrivault, S., Ishihara, H., Hoppe, I., Erban, A., Hohne, M., Moraes, T.A., Kopka, J., Szymanski, J., Nikoloski, Z., and Stitt, M. (2022). Carbon flux through photosynthesis and central carbon metabolism show distinct patterns between algae, C3 and C4 plants. *Nat Plants* 8**,** 78-91.

Wieloch, T. (2021). The next phase in the development of 13C isotopically nonstationary metabolic flux analysis. *J Exp Bot*.

Xu, G., Fan, X., and Miller, A.J. (2012). Plant nitrogen assimilation and use efficiency. *Annu Rev Plant Biol* 63**,** 153-182.

Xu, Y., Fu, X., Sharkey, T.D., Shachar-Hill, Y., and Walker, B.J. (2021). The metabolic origins of non-photorespiratory CO2 release during photosynthesis: A metabolic flux analysis. *Plant Physiol*.

Xu, Y., Wieloch, T., Kaste, J.a.M., Shachar-Hill, Y., and Sharkey, T.D. (2022). Reimport of carbon from cytosolic and vacuolar sugar pools into the Calvin–Benson cycle explains photosynthesis labeling anomalies. *Proceedings of the National Academy of Sciences* 119.

Young, J.D., Allen, D.K., and Morgan, J.A. (2014). "Isotopomer measurement techniques in metabolic flux analysis II: mass spectrometry," in *Methods Mol Biol*.), 85-108.

Zhang, Y., and Fernie, A.R. (2018). On the role of the tricarboxylic acid cycle in plant productivity. *J Integr Plant Biol* 60**,** 1199-1216.

Zhang, Y., Giese, J., Kerbler, S.M., Siemiatkowska, B., Perez De Souza, L., Alpers, J., Medeiros, D.B., Hincha, D.K., Daloso, D.M., Stitt, M., Finkemeier, I., and Fernie, A.R. (2021). Two mitochondrial phosphatases, PP2c63 and Sal2, are required for posttranslational regulation of the TCA cycle in Arabidopsis. *Mol Plant* 14**,** 1104-1118.

Table 1. Molecular ions selected for Carbon Isotopologue Distribution analysis of organic and amino acid TMS-derivatives by GC-MS.

Compounds	TMS derivative		Loss		Molecular ion		
	Formula	mass	Formula	mass	Formula	m/z	Carbon skeleton
Organic acids							
Citrate(4TMS)	C18H40O7Si4	480	CH3	15	C17H37O7Si4	465	1-2-3-4-5-6
Citrate(4TMS)	C18H40O7Si4	480	TMS-CO2, TMS-OH	207	C11H21O4Si2	273	1-2-3-4-5
Fumarate(2TMS)	C10H20O4Si2	260	CH3	15	C9H17O4Si2	245	1-2-3-4
Malate(3TMS)	C13H30O5Si3	350	CH3	15	C12H27O5Si3	335	1-2-3-4
Malate(3TMS)	C13H30O5Si3	350	TMS-CO2	117	C9H21O3Si2	233	2-3-4
Pyruvate(MEOX)(TMS)	C7H15NO3Si	189	CH3	15	C6H12NO3Si	174	1-2-3
Succinate(2TMS)	C10H22O4Si2	262	CH3	15	C9H19O4Si2	247	1-2-3-4
Amino acids							
Asparagine(2TMS)	C10H24N2O3Si2	276	TMS-CO2	117	C6H15N2OSi	159	2-3-4
Asparagine(3TMS)	C13H32N2O3Si3	348	TMS-CO2	117	C9H23N2OSi2	231	2-3-4
Aspartate(2TMS)	C10H23NO4Si2	277	TMS-CO2	117	C6H14NO2Si	160	2-3-4
Aspartate(3TMS)	C13H31NO4Si3	349	TMS-CO2	117	C9H22NO2Si2	232	2-3-4
Glutamate(3TMS)	C14H33NO4Si3	363	TMS-CO2	117	C10H24NO2Si2	246	2-3-4-5
Glutamine(3TMS)	C14H34N2O3Si3	362	TMS-CO2	117	C10H25N2OSi2	245	2-3-4-5
Glycine(3TMS)	C11H29NO2Si3	291	TMS-CO2	117	C7H20NSi2	174	2
Isoleucine(2TMS)	C12H29NO2Si2	275	TMS-CO2	117	C8H20NSi	158	2-3-4-5-6
Leucine(2TMS)	C12H29NO2Si2	275	TMS-CO2	117	C8H20NSi	158	2-3-4-5-6
Lysine(4TMS)	C18H46N2O2Si4	434	TMS-CO2	117	C14H37N2Si3	317	2-3-4-5-6
Methionine(2TMS)	C11H27NO2SSi2	293	TMS-CO2	117	C7H18NSSi	176	2-3-4-5
Ornithine(4TMS)	C17H44N2O2Si4	420	none		none		1-2-3-4-5
Phenylalanine(2TMS)	C15H27NO2Si2	309	TMS-CO2	117	C11H18NSi	192	2-3-4-5-6-7-8-9
Phenylalanine(2TMS)	C15H27NO2Si2	309	C7H7	91	C8H20NO2Si2	218	1-2
Proline(2TMS)	C11H25NO2Si2	259	TMS-CO2	117	C7H16NSi	142	2-3-4-5
Serine(2TMS)	C9H23NO3Si2	249	TMS-CO2	117	C5H14NOSi	132	2-3
Serine(3TMS)	C12H31NO3Si3	321	TMS-CO2	117	C8H22NOSi2	204	2-3
Serine(3TMS)	C12H31NO3Si3	321	TMS-CH2O	103	C8H20NO2Si2	218	1-2
Threonine(3TMS)	C13H33NO3Si3	335	TMS-CO2	117	C9H24NOSi2	218	2-3-4
Tryptophan(2TMS)	C17H28N2O2Si2	348	2TMS-C2H2NO2	218	C9H8N	130	3-4-5-6-7-8-9-10-11
Tryptophan(2TMS)	C17H28N2O2Si2	348	C9H8N	130	C8H20NO2Si2	218	1-2
Tryptophan(3TMS)	C20H36N2O2Si3	420	2TMS-C2H2NO2	218	C12H16NSi	202	3-4-5-6-7-8-9-10-11
Tryptophan(3TMS)	C20H36N2O2Si3	420	C12H16NSi	202	C8H20NO2Si2	218	1-2
Tyrosine(3TMS)	C18H35NO3Si3	397	C10H15OSi	179	C8H20NO2Si2	218	1-2
Tyrosine(3TMS)	C18H35NO3Si3	397	TMS-CO2	117	C14H26NOSi2	280	2-3-4-5-6-7-8-9
Valine(2TMS)	C11H27NO2Si2	261	TMS-CO2	117	C7H18NSi	144	2-3-4-5
Valine(2TMS)	C11H27NO2Si2	261	C3H7	43	C9H20NO2Si2	218	1-2
α-Alanine(2TMS)	C9H23NO2Si2	233	TMS-CO2	117	C5H14NSi	116	2-3
β-Alanine(3TMS)	C12H31NO2Si3	305	CH3	15	C11H28NO2Si3	290	1-2-3

Figure legends

Figure 1. Workflow used in this study. A GC-MS method was built with abundant molecular ions deriving from TMS-derivatives of organic and amino acids that contained a large number of informative carbons. Then this method was evaluated by using: i) chemical standards and tailor-made 13C-standards that had a predictable CID y using *E. coli* as a metabolic factory (^{13}C-PT); ii) unlabeled and ^{13}C-labeled plant samples.

Figure 2. **Evaluation of Carbon Isotopologue Distribution (CID) measurements for organic and amino acids by GC-MS using ^{13}C-PT reference samples**. **A**, Evaluation of amino acids using ^{13}C-PT protein hydrolysates. **B**, Evaluation of organic acids using ^{13}C-PT full metabolites extracts. Black bars correspond to expected CIDs and blue bars to the measured CIDs. The results are presented as the mean ± SD of four independent biological replicates. Statistical differences between predicted and measured CID for each isotopologue of each fragment are denoted with asterisks (*) and were established by considering the 95% confidence intervals of the measured CID. GC-MS fragments are denoted according to the considered metabolite, its MEOX/TMS-derivatives analyzed and the metabolite carbon backbone (for example, Glutamate_3TMS_C2C5 means that the fragment comes from Glutamate(3TMS) and contains the carbon C2-C3-C4-C5 (**Table 1**)).

Figure 3. Evaluation of the measurement accuracy for CID and mean ^{13}C enrichment at ^{13}C-PT and ^{13}C natural abundance in plants. A, CID accuracy and **B**, Mean ^{13}C enrichment for the selected TMS-derivatives of organic and amino acids using ^{13}C-PT samples. **C**, Residual mean ^{13}C enrichment measured in chemical standards, Arabidopsis seedlings and *B. napus* leaves after correction for isotope natural abundance. **D**, Isotopologue-specific biases identified at ^{13}C natural abundance for Proline, Valine and Threonine fragments. The results are presented as the mean ± SD of four independent biological replicates or independent preparations for commercial chemical standards.

Figure 4. **Dynamics of U-^{13}C-pyruvate incorporation in *Brassica napus* leaf discs exposed to light or dark conditions**. **A**, Mean fractional ^{13}C enrichment and **B**, Metabolite pool sizes. Mean fractional ^{13}C enrichment were monitored with GC-MS, while absolute quantification of organic and amino acids was performed respectively with GC-FID and HPLC-UV. The results are presented as the mean ± SD of four independent biological replicates. Statistical differences between dark and light conditions are denoted with asterisks according to a Student test (*, p-value <0.05; **, p-value <0.01; ***, p-value <0.001). The complete dataset is available in **Table S2, S3**.

Figure 5. **Fractional ^{13}C enrichment at the isotopologue level for TCA-cycle derived metabolites. A**, Light conditions and **B**, Dark conditions. The M0 isotopologue was not represented to facilitate the visualization of low-enriched isotopologues. The results are presented as the mean ± SD of four independent biological replicates. The complete dataset is available in **Table S2**.

Figure 6. **Fractional contribution of PEPc and TCA cycle to Malate and Citrate production in light and dark conditions. A**, Network reconstruction at the isotopomer level based on the isotopologues detected. **B**, Fractional contribution of PEPc and TCA cycle to Malate and Citrate production based on pathway-specific mass isotopologues/isotopomers. In the proposed network, the second ”turn” reflected the commitment of a molecule that has already experienced all reactions of the TCA cycle to another round of reactions (Orange and blue labels to compare acetyl-CoA-derived labeling from 1st and 2nd “turn”). Note that M0 istopologues of all metabolites will still continue to produce M0 istopologues at an important rate after a “turn” of the TCA cycle, given the ^{13}C-enrichment for Acetyl-CoA active pool. For these calculations, only the timepoint T4 and T6 hours were used and

pooled (metabolic steady-state and isotopic steady-state for isotopologue ratios). The results are presented as the mean ± SD of four independent biological replicates. Statistical comparison of Acetyl-CoA enrichment for light and dark conditions was performed with a Student-test, while fractional contributions were compared with an ANOVA followed by a post-hoc Tukey-HSD test (different letters indicate groups that were separated with a p-value <0.05).

Figure 7. **Fractional contribution of PDH and TCA-cycle derived decarboxylations to photosynthesis. A**, Fractional ^{13}C enrichment at the isotopologue level for Glycine and Serine. **B**, Working hypotheses to explain the photorespiratory-dependent labeling pattern of Glycine and Serine. **C**, Estimation of the fractional contribution of PDH (pyruvate dehydrogenase) and TCA-cycle CO_2 to photosynthesis with Serine (expressed in %). For these calculations, only the timepoint T4 and T6 hours were used and pooled (metabolic and isotopic steady-state requirements, assumption with $^{13}C/^{12}C$ of CO_2 released). The results are presented as the mean ± SD of four independent biological replicates. Statistical comparison of the two Serine fragments was performed with a Student-test.

Figure 8. **Proposed metabolic fluxes for TCA cycle and PEPc in light and dark conditions in *Brassica napus* leaves based on this study.** The contribution of stored citrate is unlikely to occur based on our results, while the forward cyclic mode of the TCA cycle has a higher contribution to both malate and citrate production than the PEPc. Questions remains about the exact proportion of Glutamate and Aspartate carbon backbones escaping the TCA cycle. Despite a reduction of PEPc activity in dark conditions compared to light conditions, PEPc-derived carbons show a higher commitment to Citrate production in dark conditions, thereby suggesting a higher rate of Malate import into mitochondria. PDH and TCA-cycle derived CO_2 are reassimilated by photosynthesis and may represent up to 30% of the TCA cycle metabolic flux. See Discussion for detailed explanations. TCA, Tricarboxylic acids; PEPc, Phosphoenolpyruvate carboxylase; OAA, Oxaloacetate; GDH, Glutamate dehydrogenase; GABA, Gamma-aminobutyric acid; ALAAT, Alanine:2-oxoglutarate aminotransferase; ASAT, Aspartate:2-oxoglutarate aminotransferase.

Identification of TMS-derivative mass fragments maximizing carbon backbones

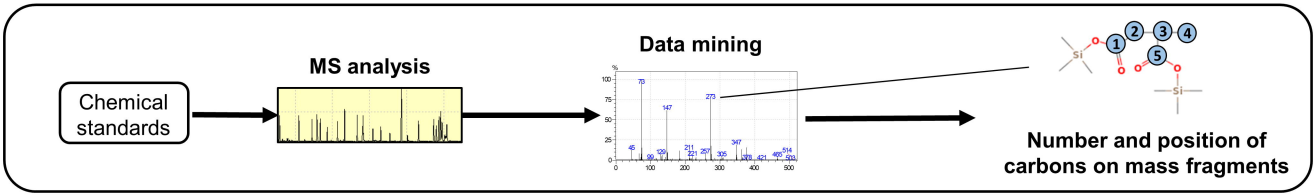

Production of reference ^{13}C labelled samples with controlled CIDs (^{13}C-PT)

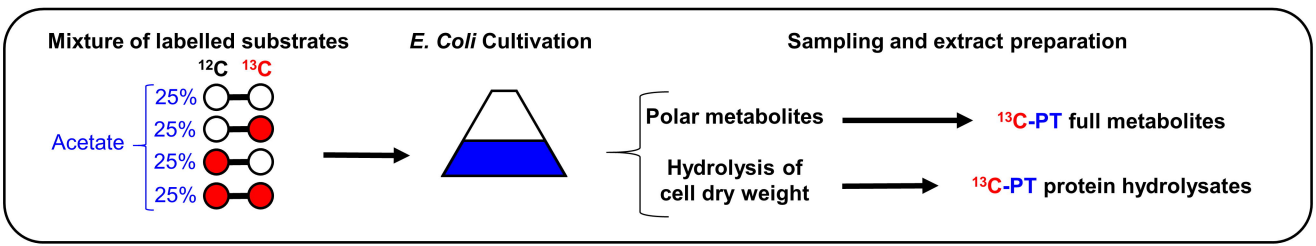

Validation of TMS-derivative mass fragments for CID measurements

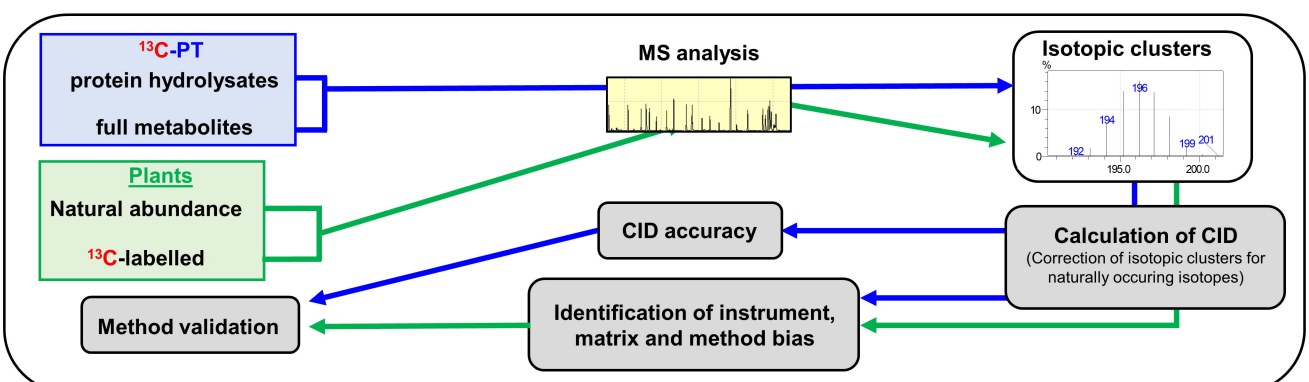

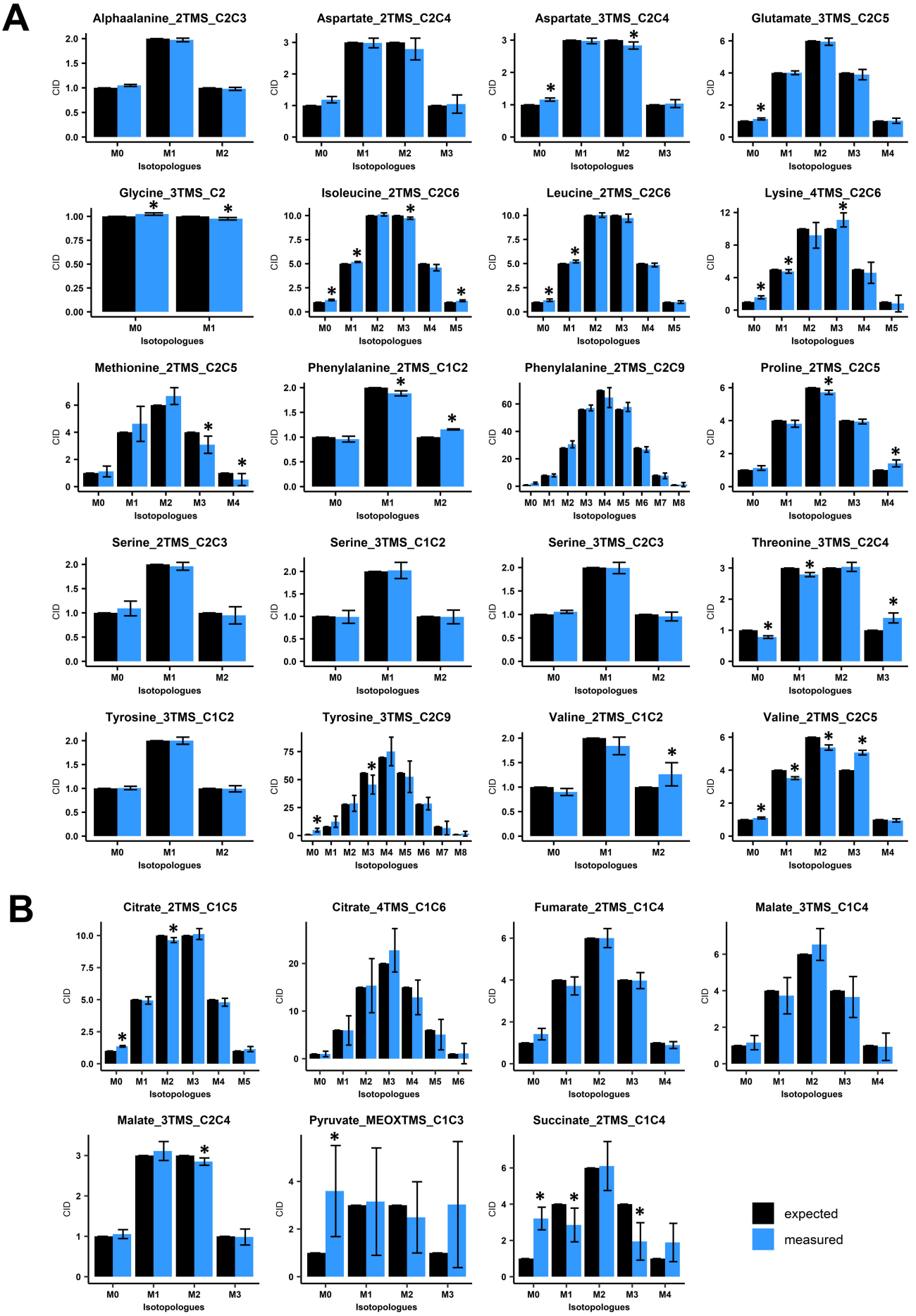
A
Alphaalanine_2TMS_C2C3
Aspartate_2TMS_C2C4
Aspartate_3TMS_C2C4
Glutamate_3TMS_C2C5
Glycine_3TMS_C2
Isoleucine_2TMS_C2C6
Leucine_2TMS_C2C6
Lysine_4TMS_C2C6
Methionine_2TMS_C2C5
Phenylalanine_2TMS_C1C2
Phenylalanine_2TMS_C2C9
Proline_2TMS_C2C5
Serine_2TMS_C2C3
Serine_3TMS_C1C2
Serine_3TMS_C2C3
Threonine_3TMS_C2C4
Tyrosine_3TMS_C1C2
Tyrosine_3TMS_C2C9
Valine_2TMS_C1C2
Valine_2TMS_C2C5
B
Citrate_2TMS_C1C5
Citrate_4TMS_C1C6
Fumarate_2TMS_C1C4
Malate_3TMS_C1C4
Malate_3TMS_C2C4
Pyruvate_MEOXTMS_C1C3
Succinate_2TMS_C1C4
CID
Isotopologues
expected
measured

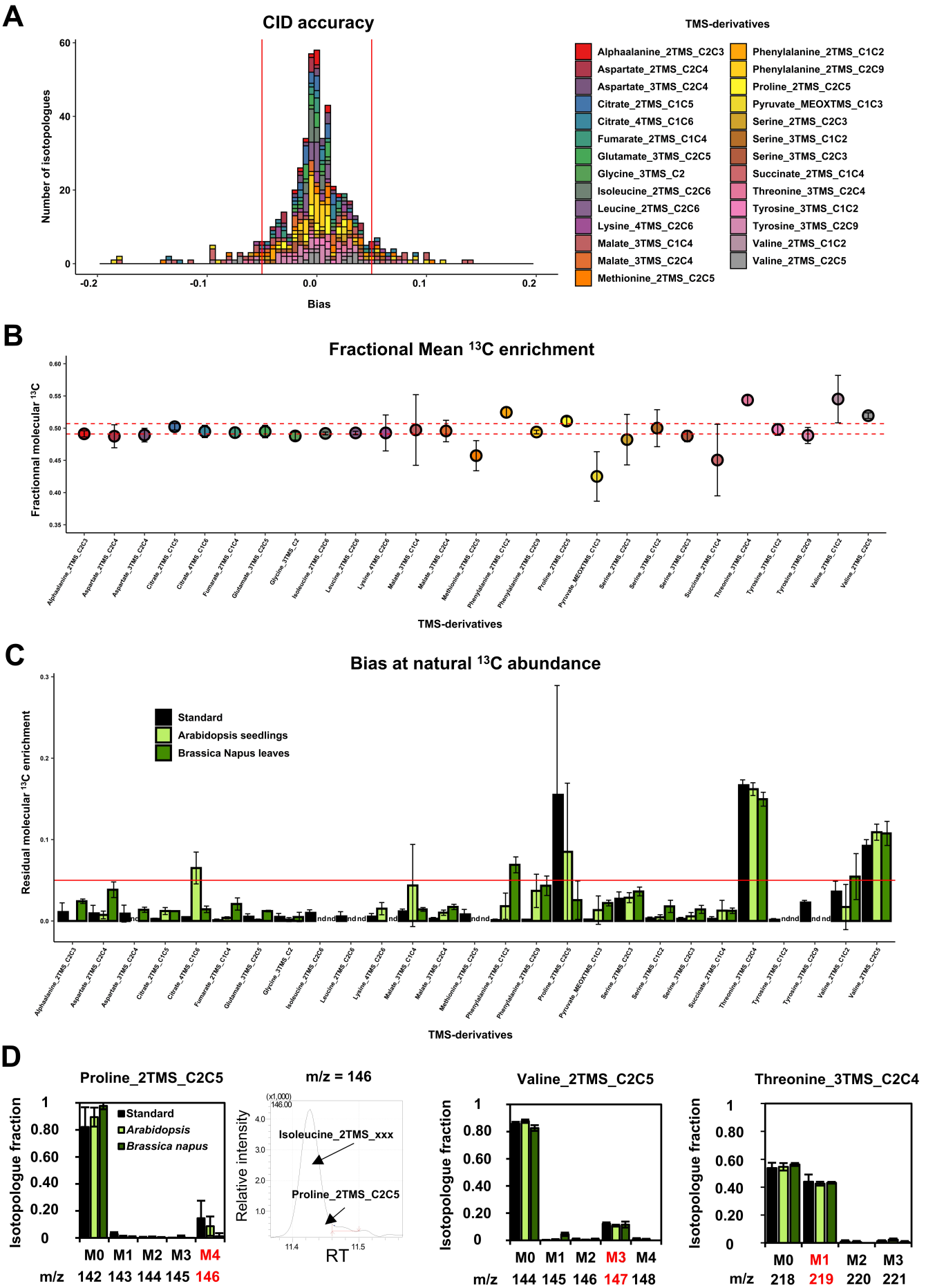
A
CID accuracy
Number of isotopologues
Bias
TMS-derivatives
Alphaalanine_2TMS_C2C3
Aspartate_2TMS_C2C4
Aspartate_3TMS_C2C4
Citrate_2TMS_C1C5
Citrate_4TMS_C1C6
Fumarate_2TMS_C1C4
Glutamate_3TMS_C2C5
Glycine_3TMS_C2
Isoleucine_2TMS_C2C6
Leucine_2TMS_C2C6
Lysine_4TMS_C2C6
Malate_3TMS_C1C4
Malate_3TMS_C2C4
Methionine_2TMS_C2C5
Phenylalanine_2TMS_C1C2
Phenylalanine_2TMS_C2C9
Proline_2TMS_C2C5
Pyruvate_MEOXTMS_C1C3
Serine_2TMS_C2C3
Serine_3TMS_C1C2
Serine_3TMS_C2C3
Succinate_2TMS_C1C4
Threonine_3TMS_C2C4
Tyrosine_3TMS_C1C2
Tyrosine_3TMS_C2C9
Valine_2TMS_C1C2
Valine_2TMS_C2C5
B
Fractional Mean 13C enrichment
Fractionnal molecular 13C
TMS-derivatives
C
Bias at natural 13C abundance
Standard
Arabidopsis seedlings
Brassica Napus leaves
Residual molecular 13C enrichment
TMS-derivatives
D
Proline_2TMS_C2C5
Standard
Arabidopsis
Brassica napus
Isotopologue fraction
M0 M1 M2 M3 M4
m/z 142 143 144 145 146
m/z = 146
Isoleucine_2TMS_xxx
Proline_2TMS_C2C5
Relative intensity
RT
Valine_2TMS_C2C5
Isotopologue fraction
M0 M1 M2 M3 M4
m/z 144 145 146 147 148
Threonine_3TMS_C2C4
Isotopologue fraction
M0 M1 M2 M3
m/z 218 219 220 221

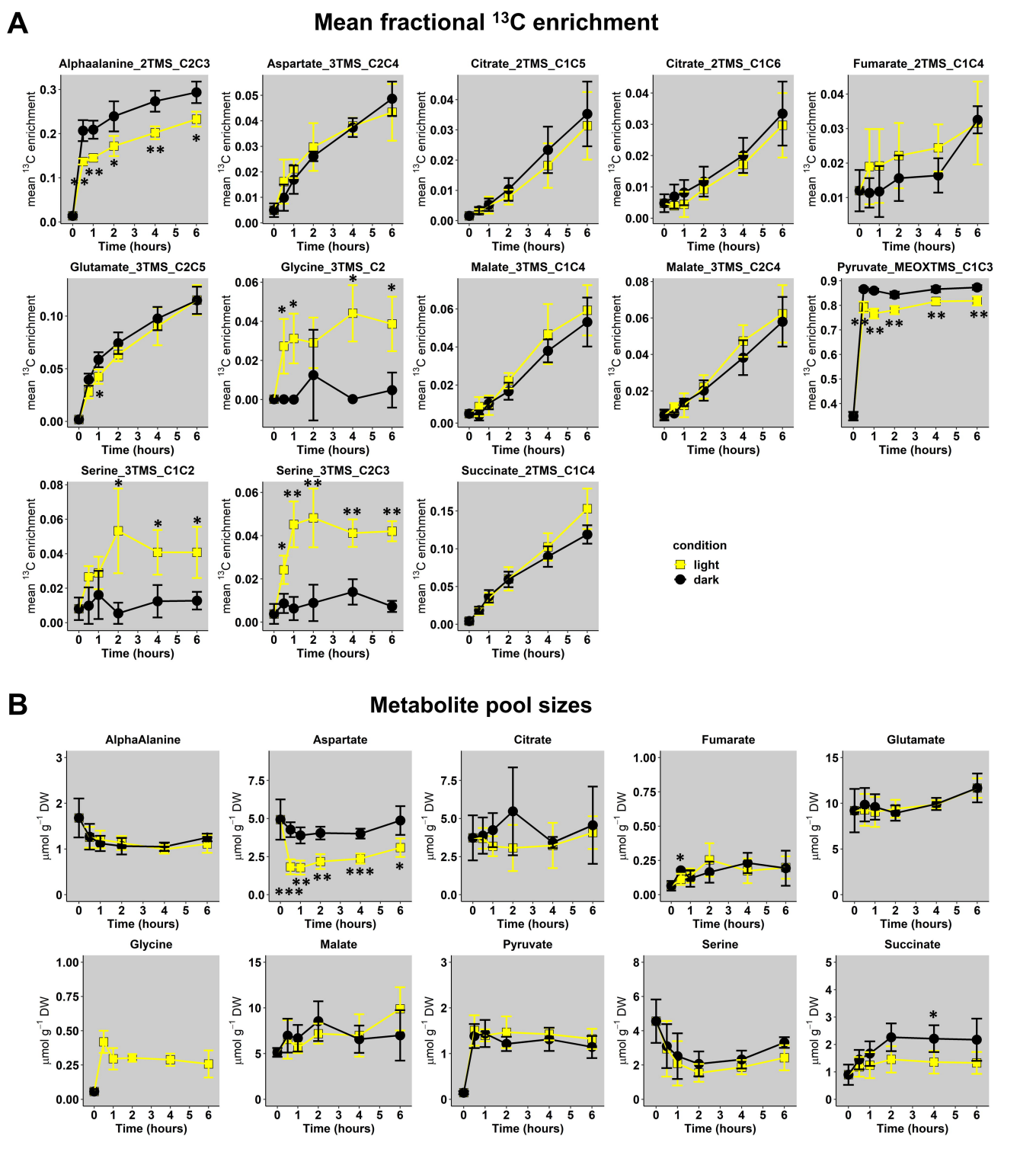
A
Mean fractional 13C enrichment
Alphaalanine_2TMS_C2C3
Aspartate_3TMS_C2C4
Citrate_2TMS_C1C5
Citrate_2TMS_C1C6
Fumarate_2TMS_C1C4
Glutamate_3TMS_C2C5
Glycine_3TMS_C2
Malate_3TMS_C1C4
Malate_3TMS_C2C4
Pyruvate_MEOXTMS_C1C3
Serine_3TMS_C1C2
Serine_3TMS_C2C3
Succinate_2TMS_C1C4
mean 13C enrichment
Time (hours)
condition
light
dark
B
Metabolite pool sizes
AlphaAlanine
Aspartate
Citrate
Fumarate
Glutamate
Glycine
Malate
Pyruvate
Serine
Succinate
µmol g−1 DW
Time (hours)

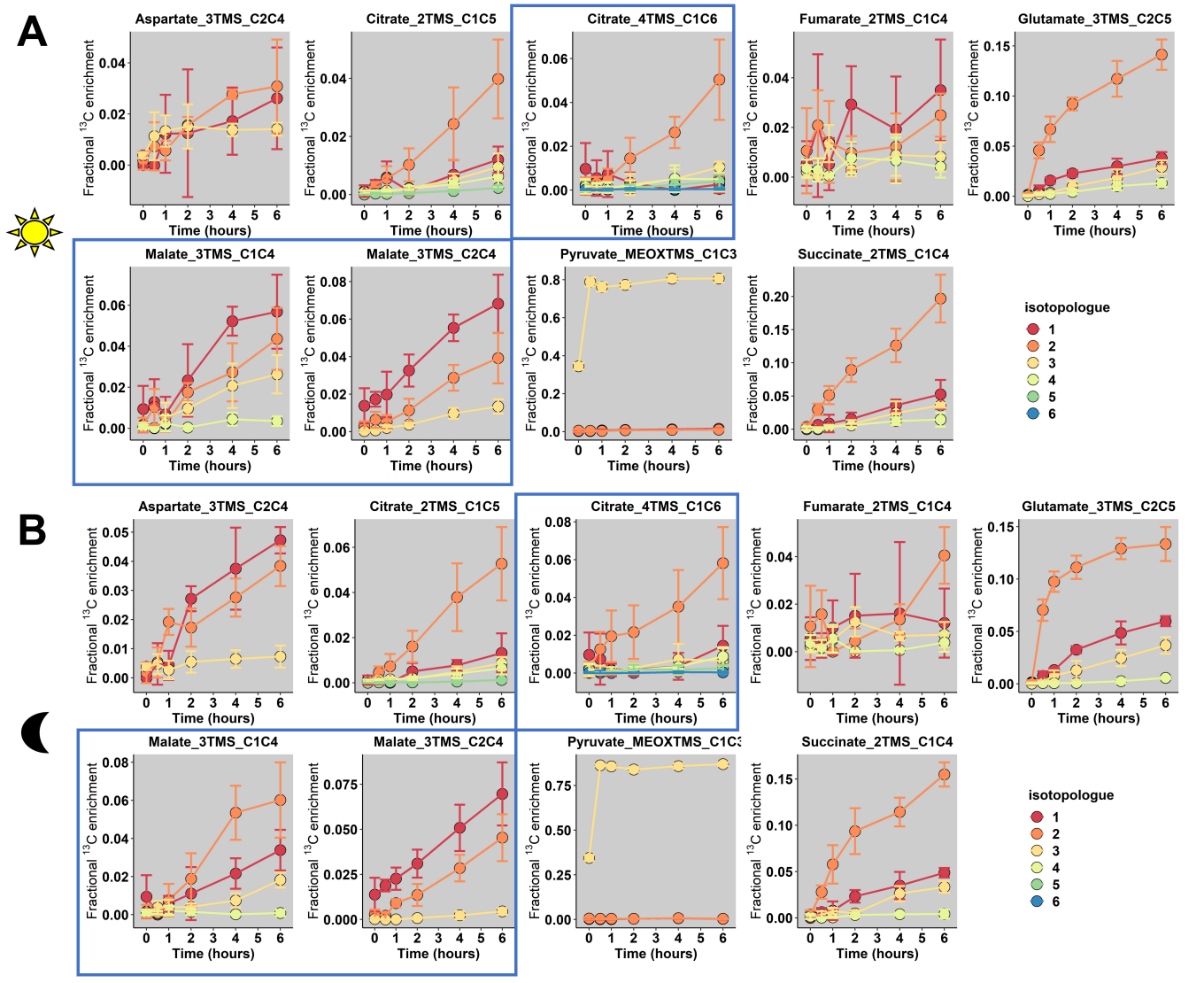
A
Aspartate_3TMS_C2C4
Citrate_2TMS_C1C5
Citrate_4TMS_C1C6
Fumarate_2TMS_C1C4
Glutamate_3TMS_C2C5
Malate_3TMS_C1C4
Malate_3TMS_C2C4
Pyruvate_MEOXTMS_C1C3
Succinate_2TMS_C1C4
Fractional 13C enrichment
Time (hours)
isotopologue
1
2
3
4
5
6
B
Aspartate_3TMS_C2C4
Citrate_2TMS_C1C5
Citrate_4TMS_C1C6
Fumarate_2TMS_C1C4
Glutamate_3TMS_C2C5
Malate_3TMS_C1C4
Malate_3TMS_C2C4
Pyruvate_MEOXTMS_C1C3
Succinate_2TMS_C1C4
Fractional 13C enrichment
Time (hours)
isotopologue
1
2
3
4
5
6

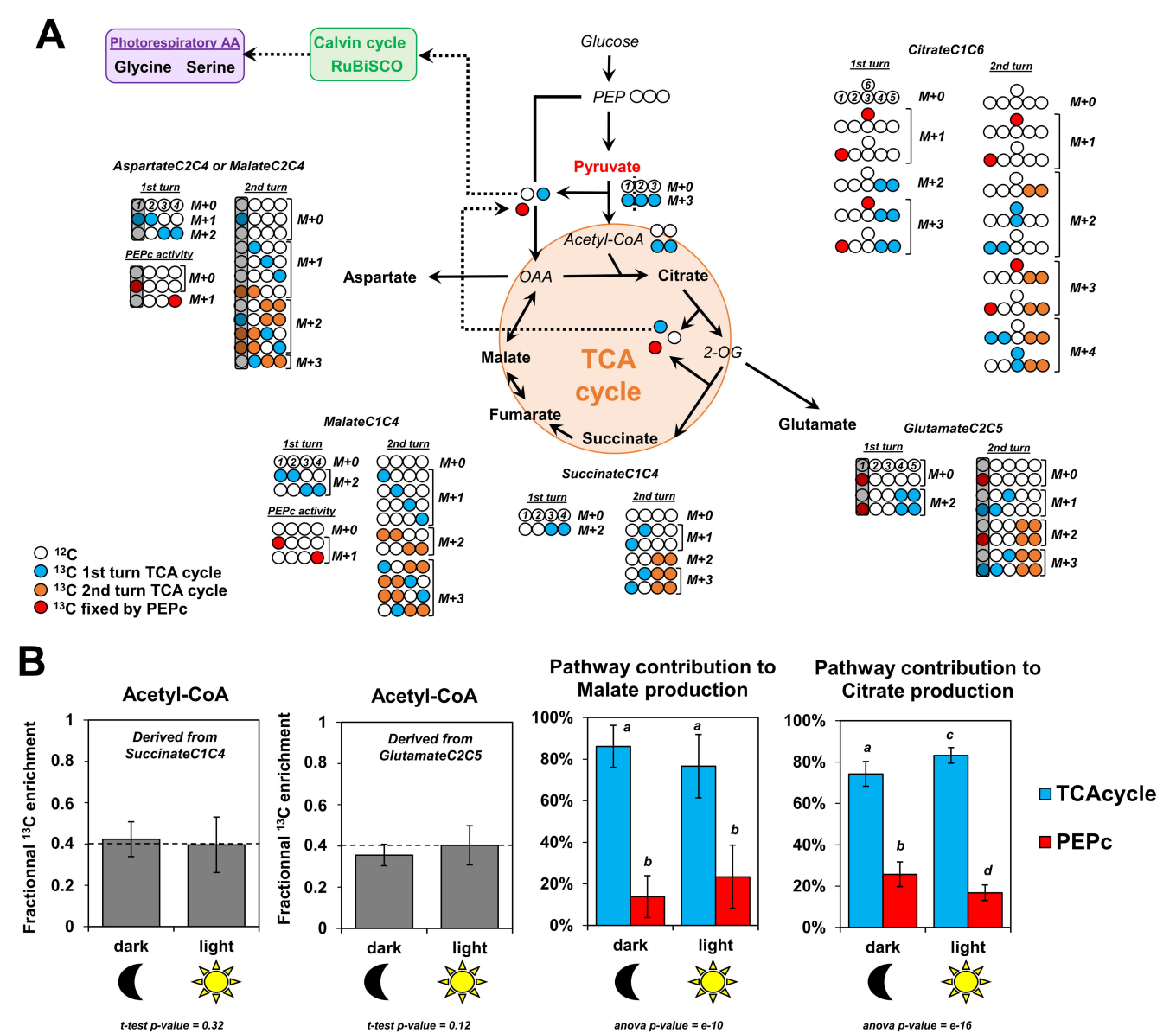
A
Photorespiratory AA
Glycine Serine
Calvin cycle
RuBiSCO
Glucose
PEP
Pyruvate
M+0
M+3
Acetyl-CoA
OAA
Citrate
Aspartate
Malate
TCA cycle
2-OG
Fumarate
Succinate
Glutamate
AspartateC2C4 or MalateC2C4
1st turn
2nd turn
PEPc activity
M+0
M+1
M+2
M+3
CitrateC1C6
M+4
MalateC1C4
SuccinateC1C4
GlutamateC2C5
12C
13C 1st turn TCA cycle
13C 2nd turn TCA cycle
13C fixed by PEPc
B
Acetyl-CoA
Derived from SuccinateC1C4
Derived from GlutamateC2C5
Fractionnal 13C enrichment
Pathway contribution to Malate production
Pathway contribution to Citrate production
TCAcycle
PEPc
dark
light
t-test p-value = 0.32
t-test p-value = 0.12
anova p-value = e-10
anova p-value = e-16

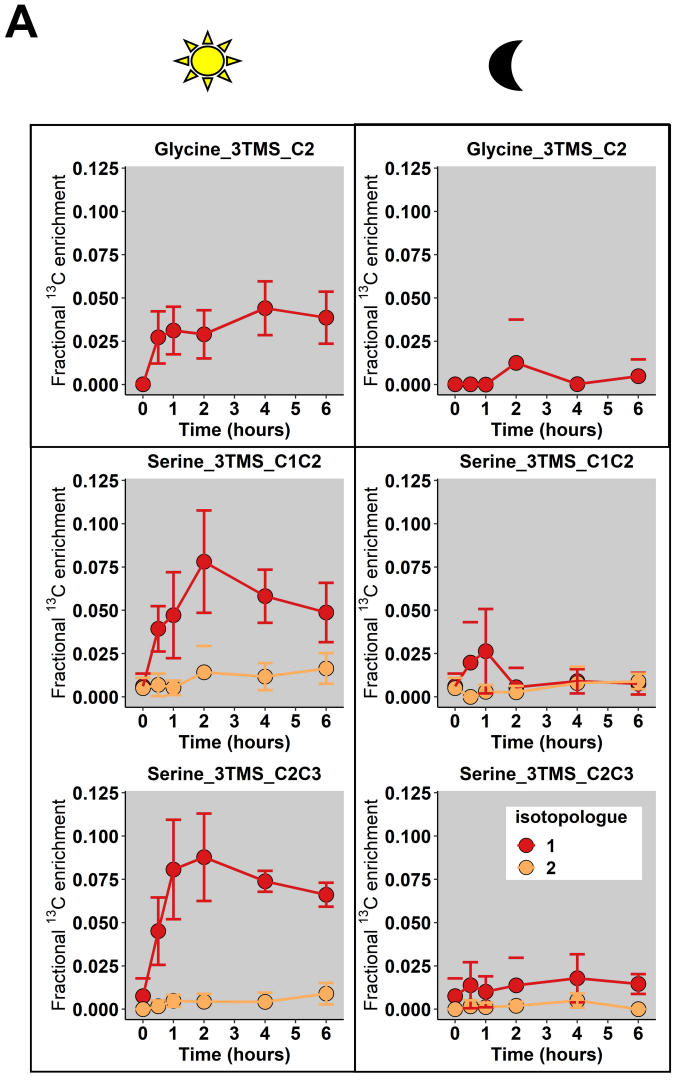
A
Glycine_3TMS_C2
Serine_3TMS_C1C2
Serine_3TMS_C2C3
Fractional 13C enrichment
Time (hours)
isotopologue
1
2

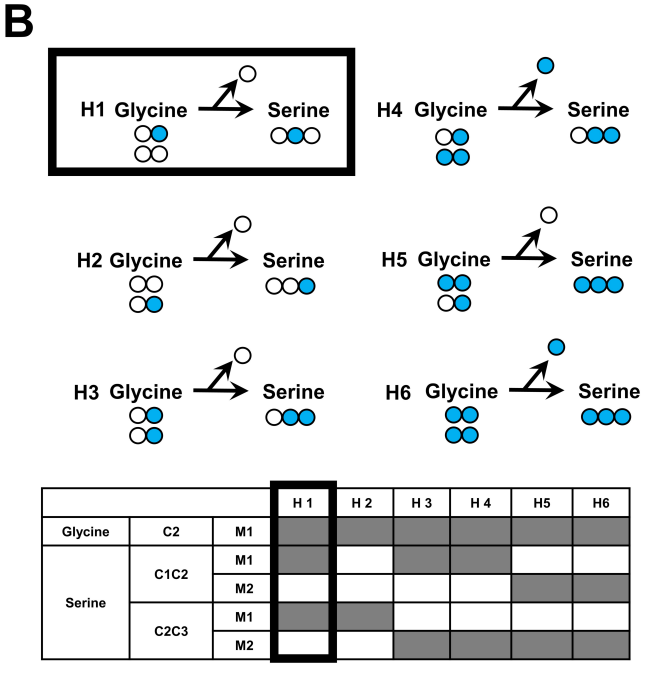
B
H1 Glycine
Serine
H2 Glycine
Serine
H3 Glycine
Serine
H4 Glycine
Serine
H5 Glycine
Serine
H6 Glycine
Serine
H 1
H 2
H 3
H 4
H5
H6
Glycine
C2
M1
Serine
C1C2
M1
M2
C2C3
M1
M2

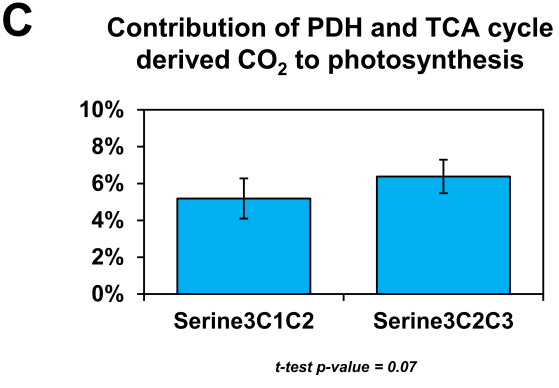
C
Contribution of PDH and TCA cycle derived CO2 to photosynthesis
10%
8%
6%
4%
2%
0%
Serine3C1C2
Serine3C2C3
t-test p-value = 0.07

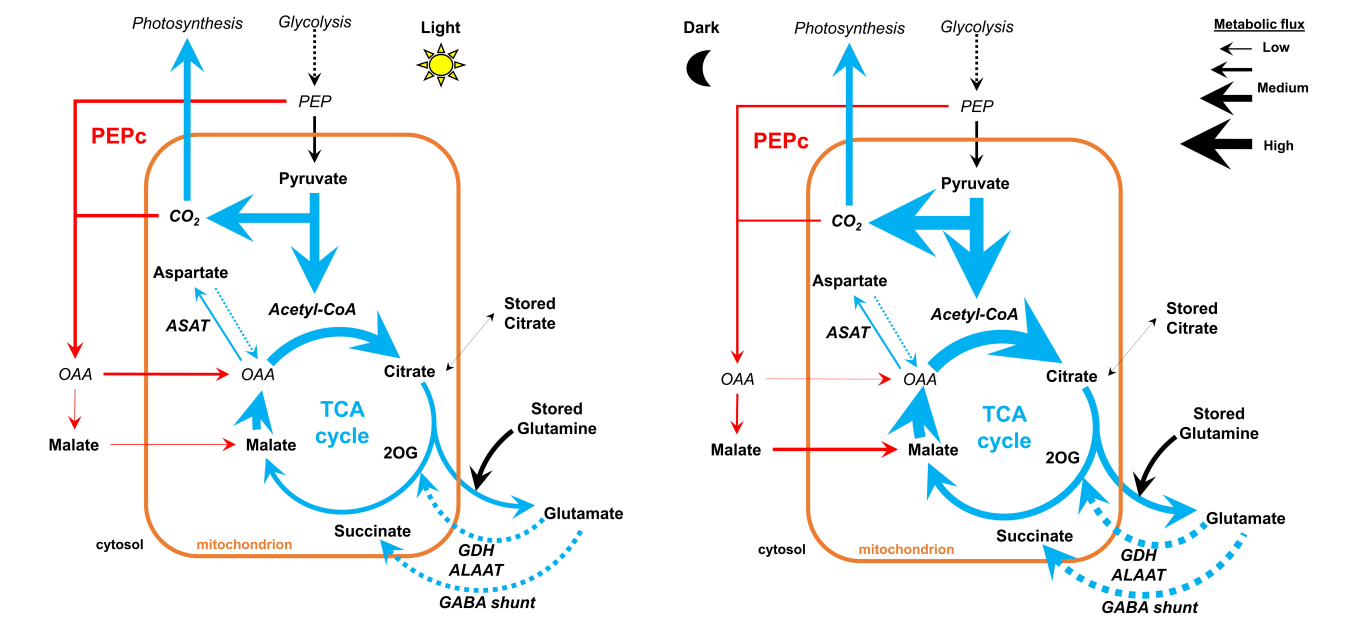
Photosynthesis
Glycolysis
Light
PEP
PEPc
Pyruvate
CO_2
Aspartate
ASAT
Acetyl-CoA
Stored Citrate
OAA
OAA
Citrate
TCA cycle
Stored Glutamine
Malate
Malate
2OG
Glutamate
Succinate
cytosol
mitochondrion
GDH
ALAAT
GABA shunt
Dark
Photosynthesis
Glycolysis
Metabolic flux
Low
Medium
High
PEP
PEPc
Pyruvate
CO_2
Aspartate
ASAT
Acetyl-CoA
Stored Citrate
OAA
OAA
Citrate
TCA cycle
Stored Glutamine
Malate
Malate
2OG
Glutamate
Succinate
cytosol
mitochondrion
GDH
ALAAT
GABA shunt